NASA CR- 151624
ERIM 130100-4-F

NASA

Final Report

SELECTION OF A SEVENTH SPECTRAL BAND FOR THE LANDSAT-D THEMATIC MAPPER

QUENTIN A. HOLMES and DANIEL R. NÜESCH
Infrared and Optics Division

JANUARY 1978

Prepared for

NATIONAL AERONAUTICS AND SPACE ADMINISTRATION
Johnson Space Center
Earth Resources Program Office
Houston, Texas 77058
Contract No. NAS9-15362
Technical Monitor: Robert K. Stewart/HA

ENVIRONMENTAL
RESEARCH INSTITUTE OF MICHIGAN
FORMERLY WILLOW RUN LABORATORIES THE UNIVERSITY OF MICHIGAN
BOX 8618 • ANN ARBOR • MICHIGAN 48107

(E78-10078) SELECTION OF A SEVENTH SPECTRAL BAND FOR THE LANDSAT-D THEMATIC MAPPER Final Report, 15 Aug. 1977 - 15 Jan. 1978 (Environmental Research Inst. of Michigan) 96 p HC A05/MF A01 CSCL 08B G3/43

N78-18487

Unclas 00078

NOTICE

Sponsorship. The work reported herein was conducted by the Environmental Research Institute of Michigan under Contract NAS9-15362 for the National Aeronautics & Space Administration, Johnson Space Center, Houston, Texas 77058. Robert K. Stewart was Technical Monitor for NASA. Contracts and grants to the Institute for the support of sponsored research are administered through the Office of Contracts Administration.

Disclaimers. This report was prepared as an account of Government sponsored work. Neither the United States, nor the National Aeronautics & Space Administration (NASA), nor any person acting on behalf of NASA:

(A) Makes any warranty expressed or implied, with respect to the accuracy, completeness, or usefulness of the information, apparatus, method, or process disclosed in this report may not infringe privately owned rights; or

(B) Assumes any liabilities with respect to the use of, or for damages resulting from the use of any information, apparatus, method, or process disclosed in this report.

As used above, "person acting on behalf of NASA" includes any employee or contractor of NASA, or employee of such contractor, to the extent that such employee or contractor of NASA or employee of such contractor prepares, disseminates, or provides access to any information pursuant to his employment or contract with NASA, or his employment with such contractor.

Availability Notice. Request for copies of this report should be referred to:

National Aeronautics & Space Administration
Scientific & Technical Information Facility
P. O. Box 33
College Park, Maryland 20740

Final Disposition. After this document has served its purpose, it may be destroyed. Please do not return it to the Environmental Research Institute of Michigan.

TECHNICAL REPORT STANDARD TITLE PAGE

1 Report No	2 Government Accession No	3 Recipient's Catalog No
ERIM 130100-4-F		

4 Title and Subtitle	5 Report Date
Selection of a Seventh Spectral Band for the Landsat-D Thematic Mapper	January 1978
	6 Performing Organization Code

7 Author(s)	8 Performing Organization Report No
Quentin A. Holmes and Daniel R. Nuesch	130100-4-F

9 Performing Organization Name and Address	10 Work Unit No
Environmental Research Institute of Michigan Infrared & Optics Division P. O. Box 8618 Ann Arbor, Michigan 48107	Task 1
	11 Contract or Grant No NAS9-15362
	13 Type of Report and Period Covered Final Report 15 Aug 77 - 15 Jan 1978
12 Sponsoring Agency Name and Address National Aeronautics & Space Administration Johnson Space Center Earth Resources Program Office Houston, Texas 77058	14 Sponsoring Agency Code

15 Supplementary Notes

Mr. Robert K. Stewart/HA, was the NASA Technical Monitor for this task.

16. Abstract

A study was carried out to develop recommendations for a 7th spectral band on the Landsat-D Thematic Mapper (TM). Beginning with a survey of remote sensing specialists the technical concepts supporting proposed applications were examined to identify candidate spectral bands. Two candidate bands in the near-IR (0.70-0.74 μm and a 1.2 μm centered band) were investigated for agricultural applications and two candidate bands (2.2 μm centered band and a 2nd thermal band) were investigated for geological applications. Each of these candidate bands were examined in terms of the feasibility of gathering high quality imagery from space while taking into account solar illumination, atmospheric attenuation and the signal/noise ratio achievable within the TM sensor constraints. For the 2.2 μm region and the thermal IR region inband signal values were calculated from representative spectral reflectance/emittance curves and a linear discriminant analysis was employed to predict classification accuracies. We emphasize that, unfortunately, no comparable test could be given to all the candidate bands which were suggested.

Based upon the substantial improvement (from 78% to 92%) in discriminating zones of hydrothermally altered rocks from unaltered zones, over a broad range of observation conditions, a 2.08-2.35 μm spectral band having a ground resolution of 30 meters is recommended for inclusion on the TM. Imagery from this spectral band will also be helpful for general geological mapping.

17 Key Words	18. Distribution Statement
Landsat-D Thematic Mapper Hydrothermally Altered Rocks Radiative Transfer Model Geologic Mapping Sensor Noise Vegetation Mapping Wheat Surveys	Initial distribution is indicated at the end of this document.

19 Security Classif (of this report)	20 Security Classif (of this page)	21 No of Pages	22. Price
Unclassified	Unclassified	viii + 94	

PREFACE

This final report documents a study which examined the scientific evidence for the addition of a 7th spectral band to the Landsat-D Thematic Mapper (TM). This study was performed within the Infrared and Optics Laboratory of the Environmental Research Institute of Michigan. The research covered in this report was performed under Task Order No. One of NASA Contract NAS9-15362 during the period from August - December, 1977. Mr. Robert K. Stewart of the Earth Resources Program Office at Lyndon B. Johnson Space Center, Houston, Texas was technical monitor for this task.

The work performed under this task represents a "quick response" effort in which several candidate bands proposed by members of a large "user community" were examined from the standpoint of the widespread usefulness of the resulting imagery from a spaceborne sensor. This study would have fallen far short of the intended goal without the cooperation and sharing of technical data from several research groups made possible by the good offices of the technical monitor and the Landsat-D Project Scientist Dr. Vincent Salomonson. Even then, the lack of adequate spectral measurements in certain spectral regions prevented a comparable chance from being given to each of the candidate spectral bands.

This task was conducted under the guidance of Mr. Richard R. Legault, Head, Infrared & Optics Division. Dr. Quentin Holmes was the project manager for this study. The authors wish to acknowledge the substantial contributions made to this work by Messrs.: Jerry Beard, Richard Nalepka, Robert Horvath, Bill Smith, Lester Witter, and George Lindquist of ERIM. We wish also to thank Dr. Alex Goetz and Dr. Anne Kahle of NASA/JPL for making available to us the excellent field measurement data they have laboriously gathered and analyzed over a period of several years, and Dr. Robert Vincent of Geospectra Corporation for his consultation in the

use of the thermal infrared region. Dr. Stephen Ungar and Ms. Vivien Gornitz of the Goddard Institute for Space Studies shared preliminary results from their studies with us, while Dr. John Barker and Dr. Mel Podwysocki briefed us on related activities in their groups. Thanks also go to Dr. Larry Rowan/USGS and Dr. Fred Henderson from the GEOSAT committee. Finally, thanks must also be given to the many researchers who took time out from their busy schedules to respond professionally to our telephone survey in order that the significant issues involved in the selection on a seventh band could be identified.

CONTENTS

CONTENTS (CONT.)

FIGURES

FIGURES (CONT.)

1
EXECUTIVE SUMMARY

In the planning for the Landsat-D Thematic Mapper provision was made for the incorporation of a 7th spectral band provided the increase in technical performance would justify the increased cost. The variety of possible applications combined with the diversity of professional opinions within a given application and the intense interest of a large community of users of spaceborne imagery required that an assessment be made of the underlying scientific evidence before a final recommendation was put forth.

Beginning with a review of existing ideas and an extensive literature survey by a senior researcher, a telephone survey was made of more than thirty well-known individuals who are currently active in remote sensing research to ascertain the critical issues in their discipline which needed to be considered in selecting a 7th band for the Thematic Mapper. The diversity of professional belief even within a specific application appears to be a basic characteristic of remote sensing technology. In order to ensure maximum information flow, the ground rule was adopted, that a respondent's name would not be released with their comments. To permit the validity of conflicting concepts to be assessed each respondent was asked to provide primary sources (based upon their current work whenever possible) which would substantiate key points. Based upon a consensus of the people interviewed, the following proposed spectral bands were examined in detail:

- 0.70-0.74 micrometer spectral band for agricultural applications
- 1.20 micrometer centered spectral band for forestry & agricultural applications
- 2.20 micrometer centered spectral band for geological applications
- 8.2-9.2 micrometer spectral band ("2nd thermal band") for geological applications.

Each of these were examined in terms of the feasibility of gathering high quality imagery from space while taking into account solar illumination, atmospheric attenuation, and the expected signal/noise ratio achievable within the sensor constraints of the Thematic Mapper design. For the 2.2 μm band and the 2nd thermal band the availability of field and laboratory spectral measurements permitted the performance gains to be quantified in terms of the increase in percent correct classifications of hydrothermally altered rocks and broad classes of rock types, respectively. The technique employed to compute percent correct classification was a linear discriminant analysis applied to inband signal values. The inband signal values were calculated from representative spectral reflectance/emittance curves for specific samples. Solar illumination, atmospheric absorption and attenuation as well as sensor noise characteristics were taken into account by the radiative transfer model used to transform ground based reflectance values into the corresponding sensor signals recorded onboard a spacecraft.

We emphasize that, unfortunately, no comparable test could be given to all the candidate bands which were suggested. The absence of sufficient reflectance/emittance spectra forced us to this proceeding. Based upon analysis of the state of the art at the end of 1977 the following conclusions are drawn and recommendations are made:

1. Although technically feasible, a band in the 0.70-0.74 micrometer region is not recommended for incorporation on the Landsat-D Thematic Mapper because, at present, there is insufficient evidence to justify its inclusion.
2. Evidence for incorporating a band in the 1.2 micrometer region (there are water absorption bands at 1.15 and 1.45 micrometers) is inferential and rests upon the idea that having two observations in the near infrared plateau would permit a resolution element to be better characterized in terms of a

mixture of vegetation and soil on different soil types. This band was not selected because low detector sensitivity combined with the already high performance of the TM in agricultural applications made this spectral band a 3rd choice.

3. - A single thermal band on the Landsat-D Thematic Mapper will probably not provide the large improvement in results which is commonly expected because of the competing physical phenomena.

- Incorporation of a 2nd thermal band (8.2-9.2 micrometers) would improve classification accuracies for some general rock types. However, using the limited amount of emission spectra available, our work does not support the contention that accurate identification of rocks according to their SiO_2 content would be possible.
- In order to simplify the data processing (make the data more accessible to the user), a 90m ground resolution for the thermal band is preferable. Unfortunately, the selected numbers of detectors cannot be changed at this late date. Great care will be required in the way these thermal data are used in conjunction with the reflective bands during machine processing.
- It is recommended that a program be undertaken to collect field and laboratory spectral data spanning both the reflective and emissive portion of the spectrum so that in future studies such as this the number and location of spectral bands in the thermal region needed to do accurate identification of general rock types can be quantified.
- Because the performance of a 2nd thermal band for general geologic mapping is on the same order as that obtainable with a 2.2 μm band, this candidate spectral band is considered to be a 2nd choice.

4. Based upon the substantial improvement in mapping zones of hydrothermally altered rocks from unaltered zones under a broad range of illumination and atmospheric conditions (from 78% accuracy with the original TM bands to 92% accuracy with this band) a 2.08-2.35 micrometer spectral band having a ground resolution of 30 meters is recommended for inclusion on the Landsat-D Thematic Mapper. Imagery from this spectral band will also be helpful for general geological mapping, as well as for discrimination among various classes of vegetation with different degrees of vigor.

2

BACKGROUND AND INTRODUCTION

The current set of six Thematic Mapper spectral bands are the end result of studies* and discussions which have taken place over a period of several years. One of the most significant of these activities was the Landsat-D Thematic Mapper technical working group convened at NASA/Johnson Space Center in mid-1975. Four panels, each composed of a number of remote sensing specialists with a variety of backgrounds were asked to independently develop recommended specifications for the Thematic Mapper with the understanding that the primary application for this sensor would be agriculture. Three out of four of these panels came in with recommendations for the allocation of two spectral bands to the near infrared reflection plateau (0.74-1.3 micrometers) of vegetation. The remaining spectral bands were allocated to the green and red portion of the visible region, the atmospheric window near 1.65 micrometers and the thermal infrared region around 11 micrometers. Based upon their understanding of the needs of potential users a spatial resolution of 30-40 meters ground IFOV combined with a radiometric accuracy on the order of 0.5% NE$\Delta\rho$ (noise equivalent change in ground reflectance) was recommended for all of the reflective bands except the 1.65 micrometer band where only a 1% NE$\Delta\rho$ was achievable. For the thermal band the recommended radiometric sensitivity was 0.5^{o}K NEΔT (noise equivalent change in ground temperature) although it was clear that this would probably only be achieved at the expense of accepting a larger ground IFOV for this band than for the other spectral bands.

In subsequent work the precise locations and spectral bandwidths were chosen in such a manner than the two bands allocated to the near infrared region were placed side by side (0.74-0.80 and 0.80-0.91 micrometers, respectively). Not surprisingly, these two bands were

*EOSPDG, 1973, Thompson, F. et al; 1974, Honeywell Radiation Center; 1974, Harnage, J.; 1975, Malila, W. et al; 1976, Morgenstern, J.; 1976, CORSPERS.

shown to have extremely high correlation ($R^2 = 0.99$) over all the data sets developed in an ERIM study (Malila, et al, 1976) which sought to quantify the expected performance of the Thematic Mapper through simulations based upon high quality aircraft imagery. Because two spectral bands with such extreme correlations are redundant, they were later combined and a new spectral band in the blue region was chosen. At that time many remote sensing specialists regarded this new spectral band (0.45-0.52 micrometers) as useful primarily for hydrological applications and research. However, a detailed study (Morgenstern et al, 1976) in the Spring of 1976 showed that to achieve high classification accuracies with maximum likelihood processing over agricultural scenes each of the five reflective bands on the Thematic Mapper would be important at some time during the growing season. In that study, TM band 1 was found to be more important than either TM band 3 or the 120 meter resolution thermal band when identifying corn and soybeans in mid-July.

In the Fall of 1976 the National Research Council's Committee on Remote Sensing Programs for Earth Resources Surveys (CORSPERS) completed an indepth review of the Thematic Mapper as the follow-on sensor to the present multispectral scanner carried by the Landsat spacecraft. Based upon their assessment of the results of remote sensing research and the underlying science in applications ranging from Cartography, Inventorying and Assessment of Vegetation, and Land Use Management to Geology, Oceanography, Water Resources Management, and Environmental Monitoring, this group's recommendations (CORSPERS, 1976) were for only slight changes in the location and band widths of the reflective bands of the Thematic Mapper. However, in the thermal region they recommended a broader thermal band (8.8-12.6 μm as opposed to NASA's choice of 10.4-12.5 μm) to permit use of a 90 m ground IFOV for this band in place of the 120 meters selected by NASA.

Figure 1 lists the spectral bands for the Thematic Mapper which were put forth by NASA shortly after the Landsat-D technical working group in 1975, the bands recommended by CORSPERS in the Fall of 1976, and the spectral bands currently specified for this sensor.

Landsat-D Thematic Mapper Technical Working Group (mid-1975) (μm)	Early 1976 (μm)	CORSPERS (Fall 1976) (μm)	Current Thematic Mapper Sensor Specification* (μm)
	0.45-0.52	0.47-0.52	0.45-0.52
0.52-0.60	0.52-0.60	0.53-0.58	0.52-0.60
0.63-0.69	0.63-0.69	0.62-0.68	0.63-0.69
0.74-0.80 } 0.80-0.91 }	0.76-0.90	0.76-0.90	0.76-0.90
1.55-1.75	1.55-1.75	1.55-1.75	1.55-1.75
10.40-12.50	10.40-12.50	8.80-12.60**	10.40-12.50

* As of August 1977.

** Chosen to reduce ground IFOV of the thermal band from 120 meters to 90 meters.

FIGURE 1. SPECTRAL BANDS RECOMMENDED FOR THE LANDSAT-D THEMATIC MAPPER BY VARIOUS GROUPS

For completeness, we now summarize the major conclusions prior to the current study:

- Initially, the Thematic Mapper spectral bands were selected with the agricultural application in mind.
- A spatial resolution of 30 meters ground IFOV was selected in order to overcome some of the limitations of the current Landsat MSS without incurring the difficult sensor design and large data processing loads associated with an even smaller IFOV.
- In an ERIM study radiometric sensitivities poorer than:

  $NE\Delta\rho$ ~0.5% for the first four spectral bands

  $NE\Delta\rho$ ~1.0% for the 1.65 micrometer spectral band

and NEΔT ~0.5°K for the thermal band were shown to result in a significant degradation of maximum likelihood classification accuracy over agricultural regions.

- With the exception of the poor spatial resolution of the thermal band, CORSPERS found the Thematic Mapper spectral bands closely paralleled the bands they would recommend for a variety of applications. However, they too had a long list of recommendations for additional spectral bands.

The purpose of the current study is to survey the evidence which supports several candidates for a 7th band and quantify the performance gains which would be achieved if a 7th spectral band were added to the Landsat-D Thematic Mapper.

3
APPROACH

Since the Landsat-D Thematic Mapper may well fulfill a role in the 1980's quite similar to that played by the current Landsat MSS in the 1970's it is important that recommendations for any additional spectral band be based upon the best available scientific evidence. Although we began by summarizing the existing literature, the need was to go beyond the level of information available in the published literature in order to assess the significance of a potential application, and to identify the primary sources of technical data which supported the selection of a spectral band for this application. To us this required that a frank discussion be held with a number of individual scientists who are actively engaged in remote sensing research. The intent was to ascertain their professional opinions and concerns regarding the critical issues involved in the selection of a 7th band for the Thematic Mapper.

For each candidate band proposed the underlying concepts and evidence were examined, and from the large number of candidates a subset was identified for even more detailed analysis.

For this subset of candidate bands calculations were made of the noise equivalent change in radiance which could be expected under a variety of sun angle and atmospheric conditions taking into account state-of-the-art detectors and assuming current Thematic Mapper values for electronic bandwidth, number of detectors/channel, and orbital parameters. The results of these computations were then compared to the magnitude of the change in radiance, at spacecraft altitude, produced by the phenomena being detected.

For candidate bands in two of the spectral regions, representative laboratory and field spectra were used in conjunction with a radiative transfer model to produce inband radiance values under the wide range of conditions of observation for which this sensor will be utilized. These values were then digitized taking sensor noise into account and a linear discriminant analysis was used to quantify the improvement in classification accuracy obtained by addition of a candidate spectral band.

4

SURVEY OF REPRESENTATIVE REMOTE SENSING SPECIALISTS

As presented in the introduction, a senior ERIM researcher contacted a representative sample of scientists who are actively involved in remote sensing research to ascertain their professional opinions and concerns regarding the applications to be pursued, the appropriate spectral regions, and the existence of technical data which would support their suggestions. In order to permit open information flow, we adopted the ground rule that no responses would be released with the contributor's name attached. Some of the opinions obtained were in direct conflict with official agency policies and had to be handled as privileged information. This is an unusual proceeding and illustrates the tension associated with the scientific and political importance of a 7th band Thematic Mapper decision.

The different professional opinions about the usefulness of adding a specific candidate band to the Landsat-D Thematic Mapper manifested itself in comments ranging from high consent to total rejection. The different interests have clashed repeatedly to the extent that NASA's plan to extend the flow of orbital earth observation data by using the Thematic Mapper to upgrade the quality of that data has not been accepted by all scientists. Concerned about relying totally on this new sensor, they wish to maintain an MSS on Landsat-D and support a design to meet operational requirements.

With the selection of inventorying and assessment of vegetation as the primary optimization objective in mission design, the program ran the risk of not serving equally the large Landsat user community which has developed. So, after having taken into consideration a band between 0.45 and 0.52 micrometers (μm) for water research, it seems reasonable that the addition of a spectral band for geological applications would be suggested.

Even in the field of geology, two main opinions crystallized:

- One supporting a band around 2.2 μm, based upon the research of L. Rowan and A. Goetz, etc.

- The other supporting a second Thermal IR channel in the 8.0-9.0 μm wavelength region, based upon the research of R. Vincent and R. Lyon.

Figure 2 is a synthesis of professional opinions by cognizant remote sensing scientists about the possible selections of a 2.0-2.6 μm spectral band for geological remote sensing and what might be preferred as an alternative.

The consensus of these contacts with the different scientists, was that the 2.0-2.6 μm wavelength region provides information on altered zones. This application is not significant to all geologists, but very important to economic geologist looking for metals. Some of the geologists, who are more interested in lithology and structure feel hydrothermal alteration is a limited application, not specific to the Office of International Geology or developing country needs, and would prefer the thermal IR or even the current MSS. It was also pointed out quite clearly, that the worst eventuality for the geology community would be, that neither the 2.0-2.6 μm band nor the second thermal IR band will be added to the Thematic Mapper. Instead of debating about the better band the ideal solution would be to fly both, a 2.0-2.6 μm and a second thermal IR band (8.2-9.2 μm). This of course could only be accommodated in the current design by eliminating an existing band which would simply cause other problems.

	PRO	CON
2.2 µm centered band	-Enthusiastic about 2.0-2.6 µm because of Rowan's and Goetz's work. -Very important for separating chemically altered rocks -JPL's work is convincing -Won't produce apples and oranges.	-Not enthusiastic about 2.0-2.6 µm, but better than nothing -Very limited for geological mapping use. -Results are not convincing -Too broad, will produce apples and oranges.
Second Thermal IR band	-Prefers two thermal bands -Very important for quartz/calcite discrimination, silica content, provides redundancy for thermal information and temperature measurements.	-Decision on Thermal IR should wait until after we can study Landsat-C experiment. -Not enough experience, more research needed before optimum IR band can be selected.

NOTE: There were also a few scientists who believed that other wavelength regions and applications were more important such as:

- Replacement of the current 1.55-1.75 µm band by a 1.55-1.65 µm and a 1.65-1.75 µm band. This is most important to identify geological alterations.
- 2.70-3.0 µm band which provides information on quartz absorption and better discrimination of sedimentary rocks.
- Most interested in 3.0-3.5 µm or 3.0-3.15 µm region for daytime and nighttime comparisons.
- Prefer photography to either of the above. Both spectral regions need further research for geological applications.

FIGURE 2. SYNTHESIS OF PROFESSIONAL OPINIONS CONCERNING A 7TH SPECTRAL BAND ON THE LANDSAT-D THEMATIC MAPPER

5

CLOSING THE GAP BETWEEN PUBLISHED DATA AND CURRENT KNOWLEDGE

To base the recommendation for a 7th band on the best technical information available at this time, the existing literature was supplemented through meetings with groups which are currently conducting related research at NASA/JPL, and NASA/GSFC. Arrangements were also made for use of as yet unpublished technical data from the following sources:

- Earth Resources Spectral Information System (ERSIS) at ERIM
- Chevron Oil Corporation
- NASA/Jet Propulsion Laboratory (JPL)
- Geospectra Corporation
- Goddard Institute of Space Studies (GISS).

Key concepts contributed by each of these groups will be presented in subsequent sections where each candidate is treated. Specific data obtained from these sources was as follows:

- NASA/JPL provided us with a large, representative, sample of calibrated rock spectra in the 0.4-2.6 μm region. These spectra provided an excellent experimental basis for the quantitative analysis of the performance of a 2.2 μm centered band.
- Chevron Oil Corporation released rock spectra and analysis results obtained from processing M-7 aircraft imagery from the Cady Hills region of California. These results were instrumental in bringing about the re-examination (see Appendix A) of the underlying physical processes responsible for spectral structure in the 2-3 μm region.
- Geospectra contributed several, previously unpublished, thermal spectra which were used in support of the thermal studies.
- Goddard Institute of Space Studies made available the agricultural field measurement data in the 0.4-1.0 μm region used to support the 0.70-0.74 μm candidate band. They also shared with us the preliminary results obtained from digital processing of 24 channel scanner data collected over Waterpocket Fold, Utah.

- Goddard Space Flight Center briefed us on their results using 24 channel scanner data over a number of geological sites and on the spectral band selection technique they have been developing.

6
RADIATIVE TRANSFER CALCULATIONS

In order to compute the changes in radiant energy at spacecraft altitude which were associated with the discrimination of specific targets it was necessary to employ a radiative transfer model which took into account aerosol scattering and molecular absorption as well as solar illumination and viewing geometry. The model employed in making all of the computations in the current study was an extension of Turner's Radiative Transfer Model such that it provided a consistent model which is applicable to a wavelength region from 0.4 to 15 micrometers. The original model (Turner, 1974) was modified to include ozone absorption in the vicinity of 0.5 micrometers. Then, it was combined with the Aggregate Model for molecular absorption. In the process it was necessary to make some simplifying assumptions in order to permit the numerical evaluation of the integrals involved.

Heuristically, we note that due to strong forward scattering (as evidenced by the dominant peaking of the scattering phase functions in the forward direction):

the scattered path length $\approx$ the direct path length.

Hence, the solar irradiance extinction can be represented as a product of the attenuations due to atmospheric scattering and molecular absorption.

$$\tau_{total} = \tau_{scattering} \cdot \tau_{absorption} \qquad (1)$$

Moreover, under the additional assumption that the altitude distribution of scatterers and absorbers is identical, path radiance values can be computed directly. This last assumption is quite reasonable for haze levels corresponding to visual ranges greater than 13 km. This assumption is not so well taken for severe haze levels (i.e., visual ranges < 5 km) where the majority of the scatterers are concentrated in the lower portion of the atmosphere.

Figure 3 shows a typical curve of spectral radiance in units of photons sec^{-1} cm^{-2} sr^{-1} μm^{-1} at the top of the atmosphere which was calculated using this model. This particular curve is based upon the reflection/emission spectrum of a healthy deciduous tree whose temperature is 300°K. The solar zenith angle for these computations was 45° and the sensor zenith angle is 0° (i.e., looking at nadir) the atmospheric composition is characteristic of a tropical region during midday with a haze level corresponding to a visual range of 23 km (i.e., a reasonably "clear day"). A logarithmic scale was chosen for the vertical coordinate of this plot because irradiance from the sun peaks around 0.6 μm and falls off very rapidly toward longer wavelengths.

The "green peak" at 0.55 μm, the chlorophyll absorption dip in the red region from 0.67 to 0.68 μm and the high near IR plateau are all characteristic of a vegetative target. While the absorption dips at 1.15 μm, 1.45 μm, and 1.95 μm are due to atmospheric water, the dip at 1.38 μm is due to CO_2. The atmosphere is essentially opaque in the region from 2.5-2.8 μm due to a number of overlapping H_2O and CO_2 absorption bands. In the emissive region between 3 μm and 14 μm the envelope of the spectral radiance is essentially that due to emission by a gray body with an emissivity of 0.95 at 300°K with a number of atmospheric absorption bands superimposed on it. At 300°K spectral radiance due to emission from the target rises to a broad maximum at around 10 μm. In addition to apparent temperature differences some materials have reststrahlen bands which serve as a basis for discrimination in the thermal region.

In the reflective region of the spectrum our computations of inband radiance were carried out by first calculating the spectral radiance at the top of the atmosphere for two limiting situations, 100% ground reflectance and 0% ground reflectance. The total radiance, $L(\lambda)$, under a specified condition of observation when viewing a material of arbitrary spectral reflectance, $\rho(\lambda)$, is then given by,

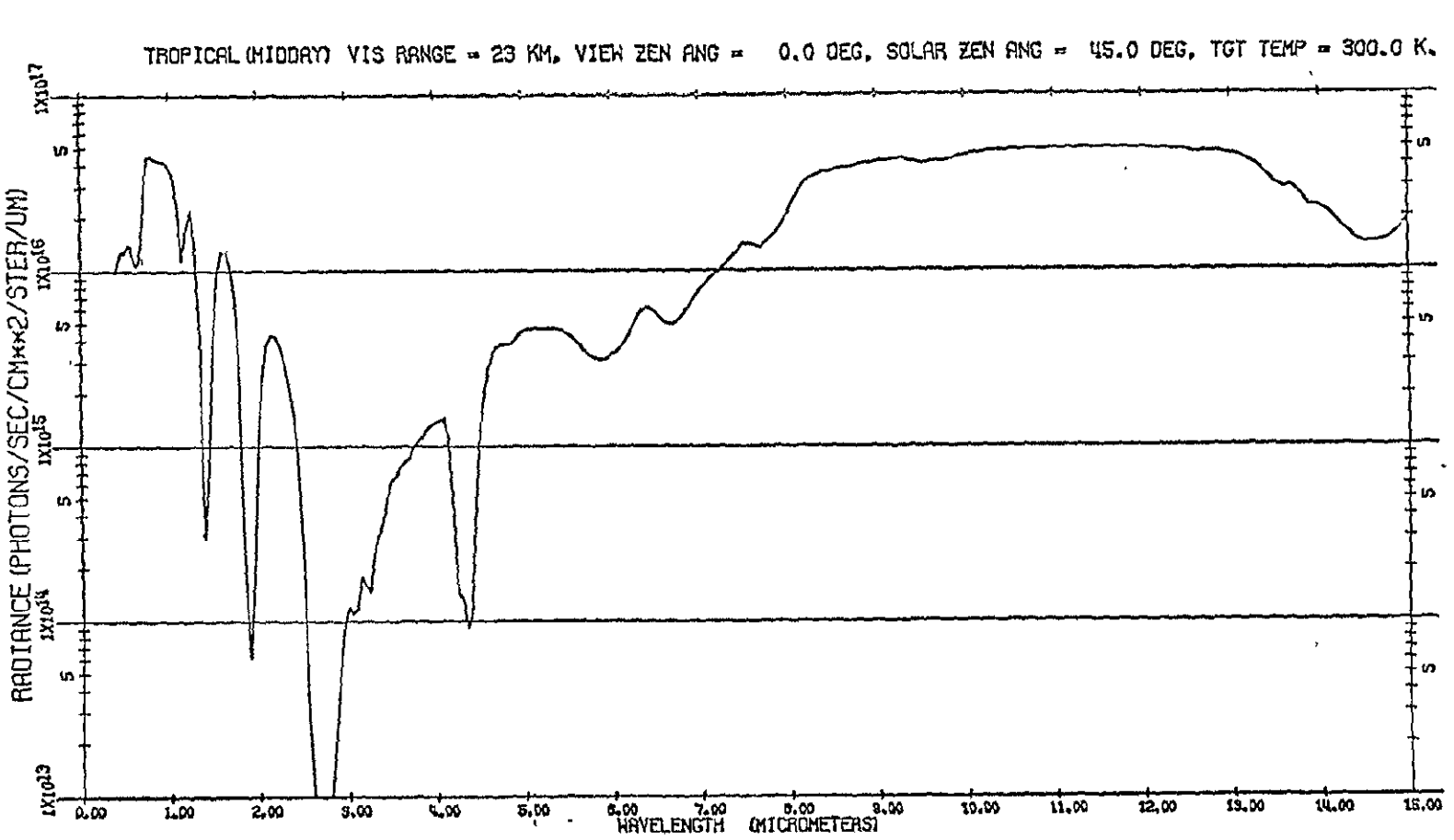

FIGURE 3. A TYPICAL CURVE OF THE RADIANCE AT THE TOP OF THE ATMOSPHERE PREDICTED BY THE RADIATIVE TRANSFER MODEL. This example was computed from the spectra of a healthy deciduous tree.

$$L(\lambda) = \frac{hc}{\lambda} \cdot \left\{ \left[t_{100}(\lambda) - t_o(\lambda) \right] \cdot \rho(\lambda) + t_o(\lambda) \right\} \qquad (2)$$

where $t_{100}(\lambda)$ and $t_o(\lambda)$ denote the total spectral radiance at the top of the atmosphere for a 100% and a 0% reflecting surface under the specific conditions of observation (i.e., $t_o(\lambda)$ represents the path radiance). The factor hc/λ (where h and c are Planck's constant and the velocity of light, respectively) converts the units from photons/sec into watts. Thus, the spectral reflectance, $\rho(\lambda)$, for a given material is transformed into the corresponding total radiance at the top of the atmosphere by a two parameter family of functions. This is illustrated in Figure 4.

In practice, both $t_{100}(\lambda)$ and $t_o(\lambda)$ are computed by numerical integration once and for all using the radiative transfer model for a specific atmospheric constitution, haze level, sun zenith angle, and sensor viewing geometry. Then Eq. (2) can be used to efficiently compute spectral radiance, $L(\lambda)$, under these same conditions for any material of whose spectral reflectance, $\rho(\lambda)$, is known.

The counterpart of Eq. (2) in the emissive region is given by,

$$L(\lambda) = \frac{hc}{\lambda} \left\{ \left[\tau(\lambda)\, L_s(\lambda) \right] \rho(\lambda) + \tau(\lambda) \left[1 - \rho(\lambda) \right] L(\tau,\lambda) + L_{path}(\lambda) \right\} \qquad (3)$$

where $L(\tau,\lambda)$ is the radiance emitted by the material being viewed on the earth's surface. This equation, which reduces to Eq. (1) when $L(\tau,\lambda)$ is negligible, is a linear equation in three parameters: solar radiance $[L_s(\lambda)]$, path radiance $[L_{path}(\lambda)]$, and radiance from the ground $[L(\tau,\lambda)]$. Hence, computations of inband spectral radiance in the thermal region must be made with the radiative transfer model for each individual material.

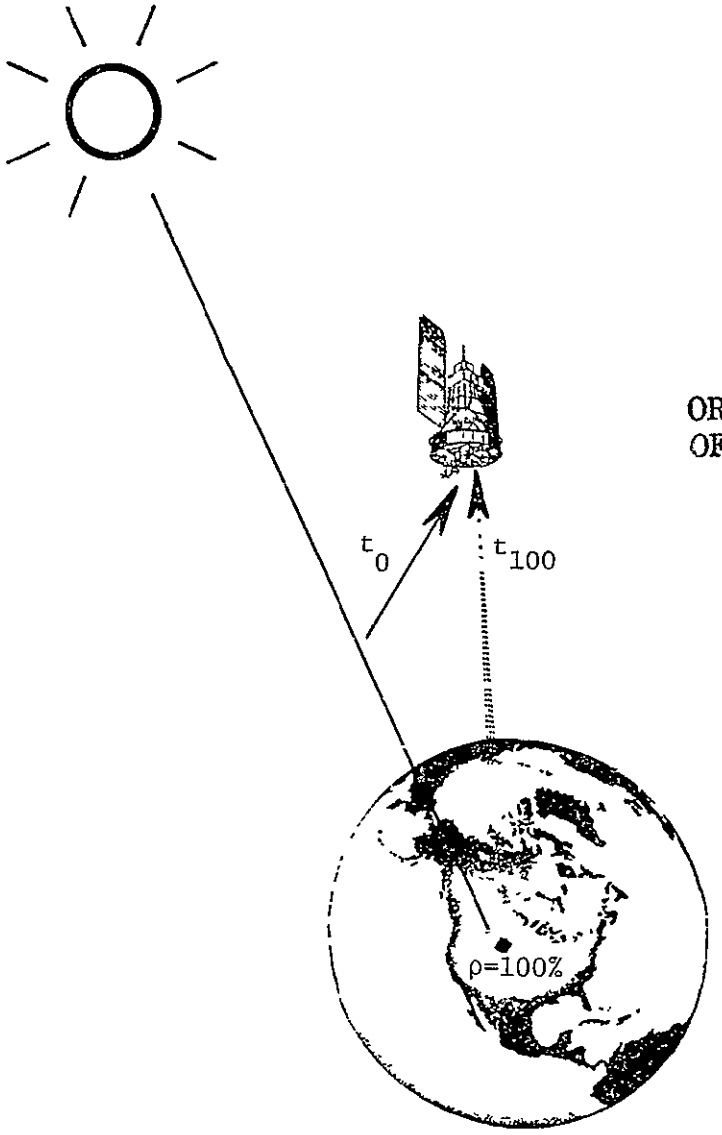

FIGURE 4. RADIATIVE TRANSFER MODEL GEOMETRY

7
ESTIMATION OF SENSOR NOISE LEVELS

One of the considerations involved in assessing the suitability of a given band for a spaceborne scanner is its noise equivalent signal level. In the course of this study estimates of the noise levels which could be expected were made for a variety of spectral bands. In all instances we assumed that the detectors employed would be individually selected, state-of-the-art devices. To allow for uncertainties in estimating the achievable values for key parameters such as transmission of the sensor optics, and detectivity of the detector, computations were made for both a pessimistic case and an optimistic case.

A straightforward development of the physics involved (See Appendix B) leads us to the well-known expression for noise equivalent power, NEP, as

$$NEP = \frac{\sqrt{B\ A_d}}{D^*} \tag{4}$$

where A_d is the area of the detector, and B is the electrical bandwidth of the sensor and D* is the detectivity of the detector. Using this equation for noise equivalent power the corresponding change in ground reflectance can be expressed in terms of the atmospheric transmission [τ_A], the sample irradiance [H_I], transmission of the optics [τ_o], and the f-number [F_N]. The resulting expression is

$$NE\Delta\rho = \frac{4F_n^2}{\tau_A H_I \tau_o D^*} \cdot \sqrt{\frac{B}{A_d}} \tag{5}$$

Equations (4) and (5) were used in conjunction with the Landsat-D Thematic Mapper parameters shown in Figure 5 to estimate sensor noise levels. Representative values for D* were chosen based upon an assessment of the state-of-the-art of detector technology by the Santa Barbara Research Center (Bode, 1976).

Orbital Altitude	705 km
Orbital Velocity	7,615 meters/sec
Swath Width	185 km
IFOV	30 meters (120 meters for the thermal band)
Detectors/channel	Channels 1-5:16 detectors, channel 6: 4 detectors

	Min Radiance (S/N)	Max Radiance (S/N)
Spectral band 1	0.28 $mW/cm^2/sr$ (32)	1.00 $mW/cm^2/sr$ (85)
Spectral band 2	0.24 $mW/cm^2/sr$ (35)	2.33 $mW/cm^2/sr$ (170)
Spectral band 3	0.13 $mW/cm^2/sr$ (26)	1.35 $mW/cm^2/sr$ (143)
Spectral band 4	0.16 $mW/cm^2/sr$ (32)	3.00 $mW/cm^2/sr$ (240)
Spectral band 5	0.08 $mW/cm^2/sr$ (13)	0.60 $mW/cm^2/sr$ (75)
Spectral band 6	300°K	320°K

FIGURE 5. NOMINAL PARAMETERS OF THE LANDSAT-D THEMATIC MAPPER

The technical difficulties associated with the machine processing of scanner imagery which has a 120 meter IFOV for the thermal band and 30 meter IFOV for the bands in the reflective portion lead the authors of this report to inquire if the number of detectors used for the thermal band could be increased to provide say 90 meter IFOV. Unfortunately, the selected number of detectors for the reflective region is not divisible by three, and the time for the major revision in the sensor design required to make this possible has long since passed.

8

CANDIDATE BAND IN THE 0.70-0.74 μm REGION

8.1 Background

Based upon a complex, mathematical investigation of scene characteristics by a group of Soviet scientists (Kondratyev, K. et al, 1975) in which the 0.70-0.74 μm region was indicated as being highly significant, a band in this region was considered as a candidate 7th band for the Thematic Mapper. A related, but considerably easier to interpret, development by an American group of scientists at Goddard Institute of Space Studies appears to support this same region for agricultural applications involving the discrimination of wheat from other agricultural crops.

8.2 Available Evidence

Seeking to identify the spectral regions most effective in characterizing remotely sensed scenes, Soviet researchers applied the mathematics of information theory to the results of remotely sensed experiments from a broad spectrum of different applications. In view of the common practice of sensor designers to avoid the shoulders of reflection peaks, many researchers were surprised when the results of this study indicated the 0.70-0.74 μm region should be intentionally included in a sensor designed to be used for agricultural applications. Even after a careful review of this work as it is reported in the literature, we can not offer a simple physical explanation as to why the 0.70-0.74 μm band was emphasized.

Based upon an interpretation of high resolution spectral radiance measurements collected over the central portions of agricultural fields in the Imperial Valley of California (Ungar, S. et al, 1977), researchers at the Goddard Institute for Space Studies believe that a narrow spectral band in this region would permit wheat in the heading stage to be distinguished from a number of other agricultural crops. Typical curves used

to support this concept in the briefing given to us by Dr. Stephen G. Ungar are shown in Figure 6. The curve labeled "Wheat" was obtained by averaging together spectral radiance curves measured while observing the interior of a single wheat field in the headed stage with a modified Jarrell-Ash 0.33 meter spectrograph mounted in a light aircraft. These "field measurements" provide digital value of radiance in 410 channels each having a bandwidth of 0.0014 μm in the spectral region from 0.43-1.0 micrometers. The difference between the spectral radiance obtained when viewing headed wheat and when viewing alfalfa is indicated by the arrows labeled "far red shift". Based upon his research, Ungar recommends using a band as narrow as possible, and no broader than 0.2 μm. For the curves shown, the largest differences occur over the region from 0.71-0.73 μm. Numerically integrating these differences over this spectral range gives a value of about 40 microwatts cm^{-2} sr^{-1}. Although this change in radiance levels is more than sufficient to be measurable at spacecraft altitudes, the results are inconclusive. The fact that these measurements of observed spectral radiance were never converted into corresponding values of spectral reflectance precludes comparisons with other curves in this atlas which were collected under different conditions of illumination. Thus, we were unable to assess the consistency of this interpretation for even the crop types which were observed in the Imperial Valley.

While there are differences of professional opinion (Private communication from C. J. Tucker, October 7, 1977) about the existence and applicability of this "far red shift" phenomena, we note that a 0.71-0.73 μm spectral band was flown on the ERIM M7 airborne scanner back in 1972. Based upon notions similar to those investigated by Stephen Ungar, this spectral band was included as a "wild card" on a flight over an agricultural region in Canada. Unfortunately, time and resources did not permit even the limited analysis to be carried out which was

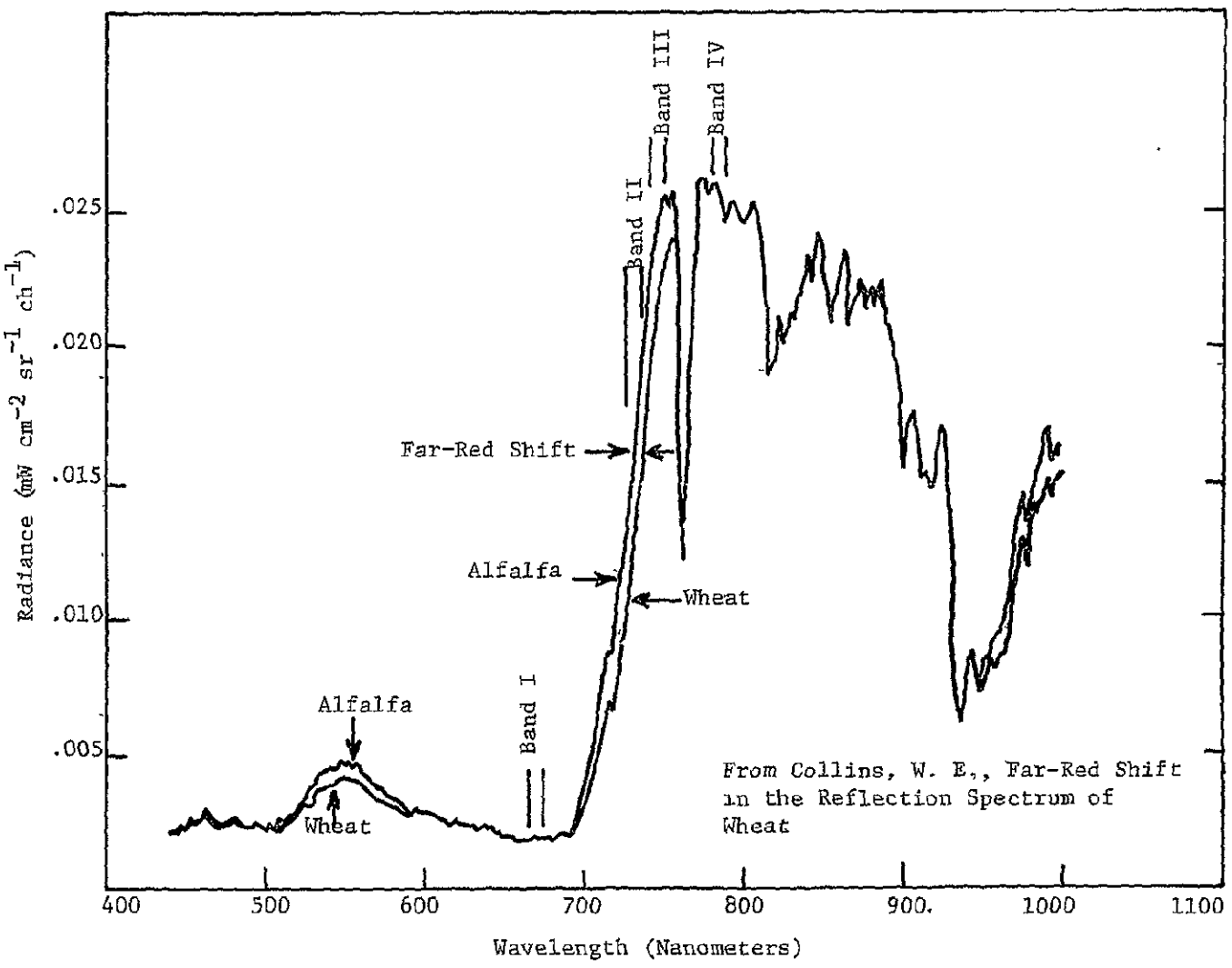

FIGURE 6. FAR RED SHIFT OF THE REFLECTION SPECTRUM OF WHEAT IN THE HEADING

originally envisioned by the researcher who suggested this band. Although collected from an aircraft, this scanner imagery has signal/noise values comparable to data which would be collected from satellite altitude with the Landsat-D Thematic Mapper. Since this imagery existed, it was examined in the course of the present study. Figure 7 shows two spectral bands (0.71-0.73 μm and 0.55-0.60 μm) collected by the M7 scanner over Guelph, Ontario in July 1972. As expected, the 0.71-0.73 μm band does not exhibit as much contrast as a spectral band which corresponds closely to TM band 2. When the appearances of several agricultural fields in the 0.71-0.73 μm spectral band were visually compared with their appearance in the 1.55-1.80 μm band and the 2.0-2.6 μm band it was clear that this band contained different information. Unfortunately, the ground truth which was collected for this flight was not suitable for use in quantifying this additional information content.

8.3 Conclusion

Although technically feasible, a spectral band in the 0.70-0.74 μm region is not recommended for incorporation on the Landsat-D Thematic Mapper because, at present, there is insufficient evidence to justify its inclusion.

(a) 0.71-0.73 μm

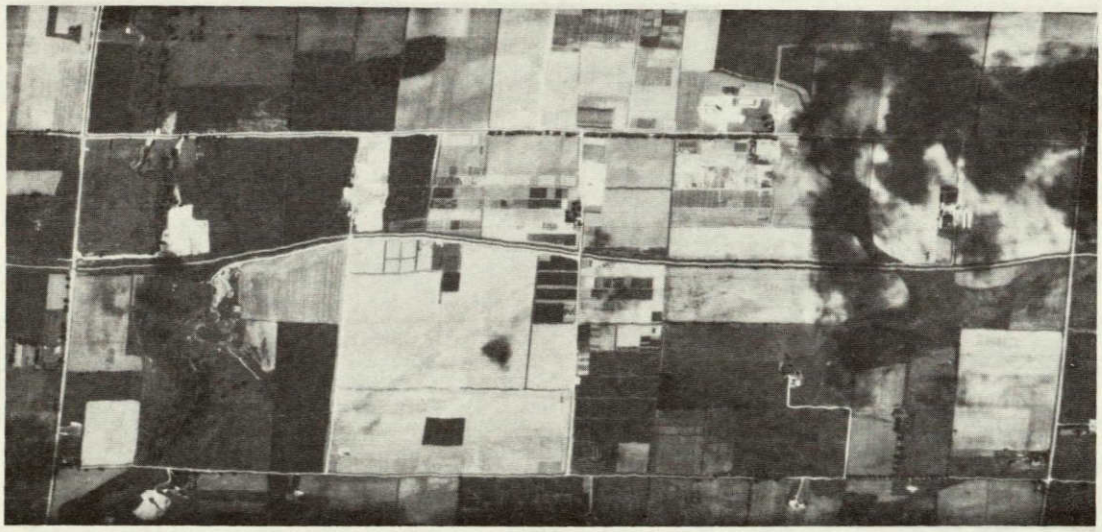

(b) 0.55-0.60 μm

FIGURE 7. ELLORA RESEARCH FARM, GUELPH, ONTARIO, CANADA
ACQUISITION DATE: 6-17-1972, ERIM M7 SCANNER

variability of spectral radiance values in this region due to different concentrations of atmospheric water can amount to as much as 30% of the nominal signals). Dr. Hoffer then pointed out that the result from this study alone was certainly not adequate to justify a conclusion. However, it did serve as another important piece in a puzzle. In his opinion, this result, in conjunction with similar results obtained during other experiments, seemed to indicate the importance of having more than one spectral band in the near IR region where vegetation has a relatively constant reflectance. More recent work at LARS (Bauer, M. E. et al, 1977) has suggested that an additional spectral band in the 1.20-1.30μm region would be useful in mapping soils in the presence of vegetation.

PbS detectors provide the highest values of detectivity in the spectral region of 1.2μm. For selected detectors it would be possible to obtain D* values of 6×10^{10} in an uncooled environment. Unfortunately, PbS detectors are not usable for this particular application because their response time is too slow. To provide a 1.2-1.3μm spectral band with a 30 meter IFOV using 16 detectors/band the need is for a detector with a bandwidth of 51.2 KHz (i.e., a time constant ~20 μsec). While PbS detectors have a time constant ranging from 5 msec (uncooled) to 0.5 msec (cooled to 77°K).

In order to meet the Thematic Mapper bandpass requirements an InAs detector cooled to 77°K would be required. This would provide a time constant ≈1 μsec and a D* value of around 3×10^{11}. Although this value of detectivity is marginal, it could be improved by cold stopping or cold filtering the detector. The corresponding noise-equivalent power, NEP, is given by:

$$NEP = \frac{\sqrt{B\ A_d}}{D^*} \tag{6}$$

using $B = 51.2 \times 10^3$ hertz, $A_d = 0.0104$ cm^2, and $D^* = 3 \times 10^{11}$ gives $NEP = 7.84 \times 10^{-12}$ watts.

Neglecting the attenuation of the radiation reflected by the ground scene as it passes from earth to the sensor and through the optical system of the sensor, the expected signal in this band from a material of 50% spectral reflectance would be 3.72×10^{-10} watts. Hence, the corresponding noise equivalent change in reflectance, $NE\Delta\rho$, would only be $\approx 2\%$.

9.4 Conclusions

Evidence for incorporating a band between 1.2 and 1.3 micrometers (there are water absorption bands at 1.15 and 1.45 micrometers) is inferential and rests upon the idea that having two observations in the near infrared would permit a resolution element to be better characterized in terms of a mixture of vegetation and soil. This band was not selected because low detector sensitivity combined with the already high performance of the TM in agricultural applications made this spectral band a 3rd choice.

10

CANDIDATE BAND IN THE 2.2 μm REGION

10.1 Background

Of particular interest to geologists is the 2.0-2.6μm region, which contains absorption bands caused by electronic processes associated with the hydroxyl radical (OH), sulfate radical (SO_4), carbonate radical (CO_3) and a few less important absorption bands in rocks and minerals (Hunt, G. R., 1977). A cellulose absorption band also occurs in this region and is thought to be useful for vegetation mapping among diseased or dead vegetation. This explains, why a number of scientists from different fields are interested in this wavelength region as a candidate for the 7th band.

For mapping limonitic altered rocks, the current 4-channel Landsat MSS sensor is very effective because it responds to the intensity of ferric-iron. The current MSS is ineffective for mapping nonlimonitic altered rocks. Also, nonhydrothermally altered limonitic rocks (such as limonitic tuffs and flows) are commonly indistinguishable from limonitic rocks. By recording multispectral images at longer wavelengths than is possible with the Landsat MSS, these limitations might be overcome (Abrams, M. J., et al, 1977).

Of greatest interest is the 2.15-2.25μm region, where nearly all altered rock spectra exhibit an intense absorption band (referred to here as the 2.2μm dip). Although the physical origins of this dip at 2.2μm are quite complex (see Appendix A) this spectral feature is largely independent of limonite content. On the other hand this 2.2μm absorption dip is absent or weak in the spectra of most unaltered rock. Figure 8 shows typical spectral reflectance curves for altered and unaltered rocks. It should be noted that the limited solar energy available in this region precludes adding a Thematic Mapper band which will unequivocally respond to this 2.2μm dip. In addition, care must be taken not to pick a spectral band which would allow the 2.35μm dip in carbonates to be confused with the 2.2μm dip of altered rocks.

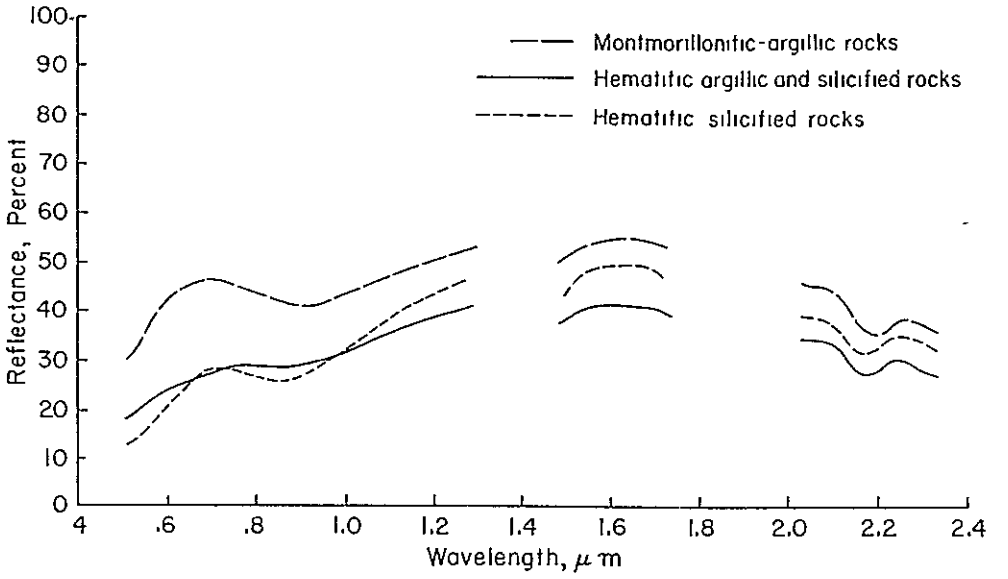

(a)

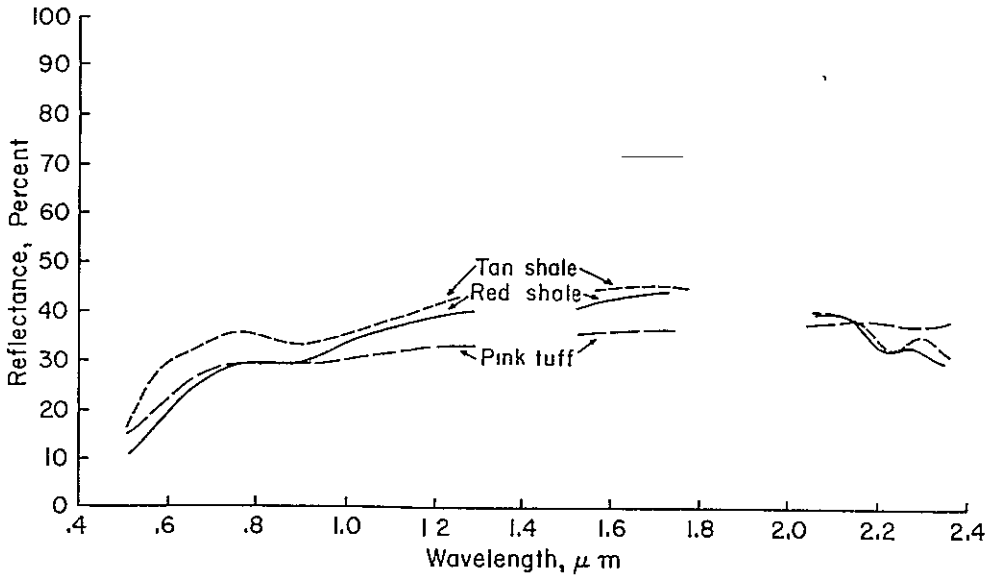

(b)

FIGURE 8. SPECTRAL REFLECTANCE CURVES OF THREE ALTERED (a) AND THREE UNALTERED (b) ROCKS FROM THE GOLDFIELD, NEVADA MINING DISTRICT (after L. Rowan et al, 1977)

For most altered rocks the reflectance maximum is at about 1.7μm; the reflectance level at 2.2μm is relatively low compared to Thematic Mapper channel 5 (1.55-1.75μm), whereas reflectances at these two wavelengths are similar for most unaltered rocks. In order to determine the usefulness of these spectral differences for discriminating non-limonitic altered rocks from unaltered rocks not only the absolute reflectances but also the ratios of the spectral bands can be analyzed.

For that reason it was ascertained by R. Vincent (1977), that it would be theoretically possible to separate altered from unaltered rocks with currently planned Landsat-D bands. He makes this statement based on an article published by L. Rowan et al, 1977 where rock and mineral samples are discussed that were collected in the Goldfield Nevada Mining District. The spectral reflectance curves shown in Figure 8 were used by Rowan to illustrate the usefulness of a 2.2μm spectral band in discriminating zones of hydrothermally altered rocks from unaltered rocks. However, as was subsequently pointed out by R. Vincent for these specific spectra it is possible to separate the three altered from the three unaltered rocks using ratios of currently planned Landsat-D spectral channels.

In response to this suggestion, recent work at NASA/JPL using a large number of representative rock spectra has shown that the current Landsat-D Thematic Mapper bands are limited in their ability to discriminate altered from unaltered rocks (J. M. Soha, private communication, September 26, 1977).

It is well known that natural vegetation can significantly mask and alter the spectral response of the ground, and so it is likely, that vegetative cover will always cause some problems in this wavelength region for geologic remote sensing. However, an additional band in this region would be quite useful for geology and would also help improve the discrimination among various classes of vegetation with different

degrees of vigor. The usefulness of a spectral band in this wavelength region might be reduced by several considerations from physical and engineering standpoints:

1. The solar irradiance at sea level ($W\ m^{-2}\mu m^{-1}$) is diminished by a factor of about 25, compared to the maximum in the green wavelength region.
2. In addition, the solar radiation and the emitted radiation from the target itself are approximately equal near the "cross-over" in the 2.0-2.6μm region. It is expected that this may result in a lower signal-to-noise ratio than could be achieved in a shorter wavelength region.
3. Since the addition of a 7^{th} channel in this wavelength region would require an independent detector dewar package, this would place a significantly increased demand on the sensor support system.

10.2 Quantification

10.2.1 Introduction

In order to provide a quantitative measure of the usefulness of a band centered near 2.2μm a linear discriminant analysis was performed on a large number of field and laboratory spectra. The majority of these spectra were provided to us by NASA/JPL through the good offices of our technical monitor. The calibrated field spectra, which were collected by NASA/JPL with a Portable Field Reflectance Spectrometer (PFRS) during the years 1974-1977 at a wide variety of sites in the Western United States, formed an excellent technical basis for this study. These, yet unpublished, spectra were grouped as shown in Figure 9.

Altered Rocks	No. of Samples
Limonitic Altered - <5% iron	10
Hematitic altered - >5% iron	87
Non-Iron Bearing Altered - bleached	13
Unaltered Rocks	
Rhyodacite	15
Andesite	29
Rhyodacite Ash Flow Tuff	10
Rhyolite Ash Flow Tuff	11
Anorthosite	20
Granite	18
Red Sandstone	8
Red-Pink Shale-Mudstone	5
Basalt	14
Coaldale Red Tuff	20
Coaldale Light Tuff	62
Argillite	12
Carbonates	29
Total Number of Samples	363

FIGURE 9. GROUPING OF ROCK SPECTRA FROM NASA/JPL

To these 363 rock spectra from NASA/JPL we added additional spectra from the NASA Earth Resources Spectral Information System (ERSIS) to assure that from a general geologic point of view all important class types were well represented. Figure 10 indicates the breakdown of the 78 additional spectra from ERSIS.

Clay Soils	2
Loam Soils	13
Sandy Soils and Sand	7
Carbonates (Minerals)	26
Carbonates (Rocks)	3
Sulphates	3
Acidic Silicate Rocks	6
Intermediate Silicate Rocks	5
Basic and Ultrabasic Silicate Rocks	6
Healthy Vegetation (Corn, Sorghum, Grass, Clover, Pine)	5
Dead Vegetation (Corn, Sorghum)	2
Total Number of Samples	78

FIGURE 10. GROUPING OF ADDITIONAL SPECTRA FROM THE EARTH RESOURCES SPECTRAL INFORMATION SYSTEM

Performing a linear discriminant analysis on the average inband reflectance values for the 363 samples from NASA/JPL we were able to discriminate the altered from unaltered rocks with an average accuracy of 78% using the current 5 TM-Bands. By including the additional band which was recommended by NASA/JPL (2.08-2.35μm), we obtained an average accuracy of 96% correct classification.

10.2.2 Candidates

As mentioned in Section 4, the different opinions of several scientists concerning the best spectral bandwidth, required more detailed examination. Different considerations had to be taken into account:

- Well positioned with regard to the different absorption bands. Candidate bands were only selected from the region between 2.0 and 2.5μm because of the atmospheric water absorption band at 1.9μm and the combined water and carbon dioxide absorption bands which make the atmosphere opaque in the region just above 2.5μm (see Figure 3).
- Bandwidth as narrow as possible relative to sensor noise.

The different candidate spectral bands (referred to here as Channels 6-13) which were investigated are shown in Figure 11.

Channel Number	Spectral Interval
Channel 6	2.08 - 2.35 μm
Channel 7	2.15 - 2.35 μm
Channel 8	2.10 - 2.35 μm
Channel 9	2.05 - 2.35 μm
Channel 10	2.10 - 2.40 μm
Channel 11	2.05 - 2.45 μm
Channel 12	2.00 - 2.40 μm
Channel 13	2.00 - 2.50 μm

FIGURE 11. CANDIDATE SPECTRAL BANDS CONSIDERED IN THE 2.2 μm REGION.

10.2.3 Transfer to a Spaceborne Sensor

To determine which of these candidate spectral bands would provide the best performance over the wide variety of conditions of observation which will be encountered by the Thematic Mapper, as it views the Earth from arctic to the tropics, computer simulations were required. First the inband radiances at the top of the atmosphere were computed for all 441 samples under a given condition of observation. Then these inband radiances were quantized in a manner which simulated the presence of sensor noise, before a linear discriminant analysis was carried out to predict the performance of a particular spectral configuration under this condition of observation. This entire procedure was repeated for several different atmospheric conditions.

10.2.3.1 Atmospheres/Conditions of Observation

For our computations we chose to use a set of seven different atmospheres/conditions of observation which are representative of the range of situations the Thematic Mapper will encounter in supporting a broad community of users. These conditions are shown in Figure 12. Cases A-F range from the excellent viewing conditions obtained when viewing the nadir at high noon through a tropical mid-day atmosphere with a visual range of 23 kilometers (case E) to the limited viewing conditions obtained when viewing the Earth at a high latitude during the winter time through a temperate mid-day atmosphere with a visual range of only 13 kilometers while the sun is 67.5° from zenith (case C). Case G was carried along only as an extreme. It corresponds to case C with the exception that visual range has been reduced from moderate haze (13 kilometers) to severe haze (5 kilometers).

	Aerosol Distribution	Visual Range	Sensor Viewing Angle	Solar Zenith Angle
Case A	Tropical	13 km	0^{o}	45^{o}
Case B	Tropical	23 km	0^{o}	45^{o}
Case C	Temperate (winter)	13 km	0^{o}	67.5^{o}
Case D	Temperate (winter)	23 km	0^{o}	67.5^{o}
Case E	Tropical	23 km	0^{o}	0^{o}
Case F	Arctic (summer)	23 km	0^{o}	45^{o}
Case G	Temperate (winter)	5 km	0^{o}	67.5^{o}

FIGURE 12. CONDITIONS OF OBSERVATION USED IN PREDICTING THEMATIC MAPPER PERFORMANCE

For the reflective region covered by TM bands 1-5 the radiative transfer model can be exercised once for each condition of observation to produce two functions, $t_{100}(\lambda)$ and $t_{o}(\lambda)$ which are then used to transform ground based values of spectral reflectance, $\rho(\lambda)$, for a sample into the corresponding spectral radiance, $L(\lambda)$, at the top of the atmosphere.

After we noted from our computations that the radiant energy emitted by a ground material at 300°K contributed less than 1% of the total radiance at the top of the atmosphere (consider Figure 3), we employed this same technique in the 2.0-2.5μm region.

For a given atmosphere/condition of observation, integration of $L(\lambda)$ for each sample across the spectral intervals corresponding to the current TM bands and the candidate bands shown in Figure 11 produced a thirteen-dimensional observation vector.

10.2.3.2 Predicted Performance Without Sensor Noise

Figure 13 and Figure 14 show the predicted performance of the Thematic Mapper in discriminating hydrothermally altered rocks from unaltered rocks for each of the candidate bands investigated under each atmosphere/condition of observation with no simulation of noise or quantization effects. These results were obtained by applying a linear discriminant analysis directly on the thirteen-dimensional inband radiance vectors of Section 2.3.1. Column 1 gives the baseline performance obtained using the five reflective bands of the current Landsat-D TM. The second through ninth columns give the percent correct classification which can be expected under this same range of observing conditions by inclusion of candidate spectral band 6 through candidate spectral band 13, respectively. The most significant item in Figure 13 (363 samples from NASA/JPL) is that the predicted performance gain is essentially the same for all candidate bands and does not even vary with the atmospheric conditions. The reason for this result is that, in the absence of sensor noise or quantization, the effect of the radiative transfer model for the reflective region is to transform the inband reflectance of each sample into a corresponding radiance value through essentially an affine transformation whose coefficients are determined by the specific condition of observation (i.e., Case A, Case B, etc.). Hence, the double precision linear discriminant analysis which was used rescaled the variables involved and achieved the same degree of separability in all cases. When the 78 additional spectra from ERSIS are included (Figure 14) there was an overall decrease in correct classification with small differences from atmosphere to atmosphere but a similar result was obtained.

To overcome this limitation the effect of sensor noise had to be taken into account.

Atmosphere/ Illumination	Spectral Channels								
	1-5	+6	+7	+8	+9	+10	+11	+12	+13
A	79.4%	95.1	96.2	95.1	95.1	95.1	95.1	94.7	94.7%
B	79.4	95.1	96.2	95.1	95.1	95.1	95.1	94.7	94.7
C	79.4	95.1	96.2	95.1	95.1	95.1	95.1	94.3	94.1
D	79.4	95.1	96.2	95.1	95.1	95.1	95.1	94.3	94.3
E	79.4	95.1	96.2	95.1	95.1	95.1	95.1	94.5	94.3
F	79.4	95.1	96.2	95.1	95.1	95.1	95.1	94.3	94.3
Mean	79.4%	95.1	96.2	95.1	95.1	95.1	95.1	94.5	94.4%
Std. Dev.	0.0%	0.0	0.0	0.0	0.0	0.0	0.0	0.18	0.24%

FIGURE 13. PREDICTED PERFORMANCE OF THE THEMATIC MAPPER IN DISCRIMINATING HYDROTHERMALLY ALTERED ROCKS FROM UNALTERED ROCKS
(Percent Correct Classification)
(No Sensor Noise -- 363 Samples)

Atmosphere/ Illumination	Spectral Channels								
	1-5	+6	+7	+8	+9	+10	+11	+12	+13
A	76.1%	93.1	93.4	93.2	93.2	92.8	92.6	92.9	92.9%
B	76.4	93.1	93.4	93.2	92.8	92.4	92.6	92.8	92.9
C	78.6	93.2	93.8	93.7	93.2	93.1	92.9	92.8	92.8
D	77.8	93.2	93.4	93.5	93.2	93.1	92.5	92.8	92.8
E	79.2	93.5	95.0	94.0	93.5	93.8	93.4	93.1	93.1
F	76.4%	92.9	93.4	93.0	92,5	92.5	92.3	92.8	92.8%
Mean	77.40%	93.17	93.73	93.43	93.07	92.95	92.72	92.87	92.88%
Std. Dev.	1.31%	0.20	0.64	0.37	0.36	0.51	0.39	0.12	0.12%

FIGURE 14. PREDICTED PERFORMANCE OF THE THEMATIC MAPPER IN DISCRIMINATING HYDROTHERMALLY ALTERED ROCKS FROM UNALTERED ROCKS
(Percent Correct Classification)
(No Sensor Noise -- 441 Samples)

10.2.3.3 Sensor Noise

As is well known, the performance of a sensor can be defined relative to parameters such as IFOV, spectral resolution and signal-to-noise (S/N) ratio. The noise in a sensor may arise from the radiation, the current induced by the incoming radiation, the detector itself or the detector electronics but the predominant source is dependent upon the detector and its operating conditions.

For the reflective region the noise equivalent change in radiance, NEΔL, depends upon the signal level. This dependence is well represented by a function of the form:

$$NE\Delta L = \sqrt{\alpha + \beta S} \qquad (7)$$

where S is the signal level while α and β are constants which characterize respectively the dark current of the detector and the shot noise of the detector due to both the statistical nature of the local photons and the response of the detector to the incoming electromagnetic radiation.

Using the sensor performance figures (S/N ratios at the maximum and minimum radiance levels) given in the Landsat-D Thematic Mapper sensor specifications (GSFC, 1977) we calculated values for α and β for each of the existing spectral bands. Since an InSb detector was the best choice for a 2.2μm centered spectral band we used the values of α and β from the existing 1.55-1.75μm band which uses this same detector type. Figure 15 shows the values of α and β we obtained and the corresponding values of NEΔL at the expected minimum and maximum radiance levels. As can be seen, for all of these bands we are operating near the knee of the curve between a dark current limited sensor and a shot noise dominated sensor. For our computer simulation of sensor noise we used quantization levels which corresponded* to a one sigma NEΔL value of 10 μwatts cm^{-2} sr^{-1} for channels 1-4 and 7 μwatts cm^{-2} sr^{-1} NEΔL for channels 5-13.

*See Appendix C

Channel	$\Delta\lambda$	α	β	$NE\Delta L_{min\ radiance}$	$NE\Delta L_{max\ radiance}$
1	.45-52 μm	5.2511×10^{-5}	8.5897×10^{-5}	8.75 μw cm^{-2} sr^{-1}	11.76 μw cm^{-2} sr^{-1}
2	.52-.60 μm	3.0848×10^{-5}	6.7383×10^{-5}	6.86 μw cm^{-2} sr^{-1}	13.71 μw cm^{-2} sr^{-1}
3	.63-.69 μm	1.8167×10^{-5}	5.2561×10^{-5}	5.00 μw cm^{-2} sr^{-1}	9.44 μw cm^{-2} sr^{-1}
4	.76-.90 μm	1.7606×10^{-5}	4.6215×10^{-5}	5.00 μw cm^{-2} sr^{-1}	12.50 μw cm^{-2} sr^{-1}
5	1.55-1.75 μm	3.3850×10^{-5}	5.0251×10^{-5}	6.15 μw cm^{-2} sr^{-1}	8.00 μw cm^{-2} sr^{-1}
6-13	2.0-2.5 μm	3.3850×10^{-5}	5.0251×10^{-5}	6.15 μw cm^{-2} sr^{-1}	8.00 μw cm^{-2} sr^{-1}

FIGURE 15. PARAMETERS DESCRIBING THE NOISE EQUIVALENT RADIANCE LEVELS OF THE LANDSAT-D THEMATIC MAPPER CHANNELS

10.2.3.4 Predicted Performance with Sensor Noise Included

Figure 16 shows the predicted performance of the Thematic Mapper in discriminating hydrothermally altered rocks from unaltered rocks under a variety of conditions of observation with the inclusion of 1σ sensor noise. These results are based upon a linear discriminant analysis of the 441 samples obtained by simulating the effect of sensor noise after applying the radiative transfer model to the combined spectra from both NASA/JPL and the ERSIS.

For a given atmosphere/condition of observation the addition of a sixth reflective band gives an increase in the percent correct classification, with candidate spectral bands 8, 9, 10, and 11 giving generally lower performance than spectral bands 6 (2.08-2.35μm), candidate 7 (2.15-2.35 μm), or candidate 13 (2.00-2.50 μm).

To understand better why four of the seven candidate bands performed significantly poorer than the remaining three candidate bands we determined which spectra were being misclassified. Inspection revealed that the majority of this difference in performance was due to a large proportion of the Non-Iron bearing altered rocks, the Coaldale Red Tuff, and the Coaldale Light Tuff being consistently misclassified when one of these four spectral bands were used.

Because the goal was to select a spectral band which gave the best possible performance over a wide range of conditions of observation we used the mean classification accuracy over all six atmosphere/illumination conditions as our figure of merit. In order to ascertain the dependence of these results on the noise level which was modeled, we repeated all the computations twice more:

- Noise Level ≈ σ/3
- Noise Level ≈ 3σ

The results of these simulations are given in Figure 17.

Atmosphere/ Illumination	Spectral Channels 1-5	+6	+7	+8	+9	+10	+11	+12	+13
A	77.4 %	93.4	90.4	86.1	85.5	86.7	81.4	89.4	92.3 %
B	76.7	93.8	91.3	83.7	84.4	87.1	82.4	89.0	92.6
C	77.1	89.6	89.4	82.3	83.7	85.3	81.4	88.7	89.8
D	77.8	88.5	88.8	83.4	85.9	86.5	82.6	89.8	90.1
E	79.5	93.8	92.9	82.0	84.0	86.1	82.2	92.0	92.3
F	77.0	91.4	92.2	85.2	84.6	87.6	81.6	91.9	90.8
Mean	77.75%	91.75	90.83	83.78	84.68	86.55	81.97	90.05	91.32%
Std. Dev.	1.01%	2.30	1.60	1.61	0.86	0.80	0.53	1.56	1.24%

FIGURE 16. PREDICTED PERFORMANCE OF THE THEMATIC MAPPER IN DISCRIMINATING HYDROTHERMALLY ALTERED ROCKS FROM UNALTERED ROCKS
(Percent Correct Classification)
(1σ Noise Level -- 441 Samples)

	Spectral Configuration								
	Channels								
	1-5	+6	+7	+8	+9	+10	+11	+12	+13
σ/3 Noise Level									
Mean	77.47%	93.93	94.17	93.90	93.80	93.65	93.72	93.53	93.43%
Std. Dev.	0.98%	0.45	0.36	0.45	0.38	0.55	0.90	0.48	0.33%
3σ Noise Level									
Mean	75.81%	80.35	81.27	78.43	80.78	79.38	79.27	84.20	84.75%
Std. Dev.	1.83%	4.27	4.55	2.64	1.71	2.83	1.29	3.72	4.22%

FIGURE 17. SENSITIVITY OF PREDICTED THEMATIC MAPPER PERFORMANCE TO SYSTEM NOISE; HYDROTHERMALLY ALTERED ROCKS FROM UNALTERED ROCKS
(Percent Correct Classification)
(441 Samples)

Our interpretation of these results is that in the presence of small noise levels ($\approx\sigma/3$) the best performance is obtained from the narrowest spectral band (Candidate #7, 2.15-2.35 μm). In the presence of high noise levels ($\approx 3\sigma$) the best performance is achieved by using the broadest spectral band (Candidate #13, 2.00-2.50 μm). For a system whose noise levels conform to the Landsat-D sensor specification ($\approx 1\sigma$) the 2.08-2.35 μm band is optimum followed closely by the 2.00-2.50 μm band. Since the primary physical phenomena being exploited is the 2.2 μm dip in the reflection spectra of hydrothermally altered rocks, we opted for the first of these two candidates on the grounds that all other things being equal, a narrow spectral band will provide results which are more unequivocal.

10.2.3.5 Additional Investigations

One of the technical concerns about a 2.2 μm centered band was the influence of the carbonates, i.e., would carbonates become confused with hydrothermally altered rocks. To answer this question we examined the performance on a special data set of 168 samples (110 hydrothermally altered samples, 29 carbonates samples from NASA/JPL and 29 carbonate rocks and minerals from ERSIS). Figure 18 shows the predicted performance of the TM in discriminating between altered rocks and carbonates in the presence of 1σ noise.

As can be seen from this table both the 2.08-2.35 μm band and the 2.00-2.50 μm band perform quite well. Considering that the carbonate absorption dip around 2.35 μm is somewhat masked by the rapid decrease in solar irradiance with increasing wavelength, it is not surprising that the broader band is slightly better and more consistent.

Atmosphere/ Illumination	Spectral Channels								
	1-5	+6	+7	+8	+9	+10	+11	+12	+13
A	80.2%	97.4	91.2	90.0	95.2	93.9	92.6	94.8	94.7%
B	80.6	94.3	92.9	91.7	96.5	95.2	91.2	93.9	92.5
C	77.5	86.8	87.8	86.8	90.3	87.3	91.2	87.7	91.7
D	76.1	86.0	88.2	86.4	87.3	86.0	92.5	90.3	90.8
E	84.6	95.5	96.0	83.8	89.5	94.8	93.9	95.6	93.8
F	81.0	92.9	92.6	92.6	95.2	95.2	93.9	93.0	95.1
Mean	80.0%	92.15	91.45	88.55	92.33	92.07	92.55	92.55	93.10%
Std. Dev.	2.97%	4.70	3.10	3.43	3.78	4.24	1.21	3.00	1.71%

FIGURE 18. PREDICTED PERFORMANCE OF THE THEMATIC MAPPER IN DISCRIMINATING HYDROTHERMALLY ALTERED ROCKS FROM CARBONATES
(1σ Noise Level -- 168 Samples)

We also checked the performance of a 2.08-2.35 μm band for general geologic purposes where not only altered rocks should be discriminated from unaltered rocks, but all rock types among themselves. This was done by applying a linear discriminant analyses to the 15 band ratios obtained for 390 samples in the presence of 1σ noise for both the best and worst condition of observation. The results are shown in Figure 19. As expected, there is a considerable improvement in performance between atmosphere C and atmosphere E because ratio processing is most appropriate when atmospheric path radiance is small. It should be noted that for general mapping the average class performance we obtained ranged between only 54% correct classification and 62% correct classification.

For completeness, we include a correlation matrix for each of the original TM bands and the candidate spectral bands considered in this section. This matrix (shown in Figure 20) was computed for atmosphere E and a 1σ noise level over all 441 sample spectra.

10.3 Conclusions

Based upon the substantial improvement in mapping zones of hydrothermally altered rocks from unaltered zones over a broad range of illumination and atmspheric conditions, a 2.08-2.35 μm spectral band having a ground resolution of 30 meters is recommended for inclusion on the Landsat-D Thematic Mapper. Imagery from this spectral band will also be helpful for general geologic mapping; as well as for discrimination among various classes of vegetation with different degrees of vigor.

Sample	Number	Percent Correct Classification: Worst Case (Atmosphere C)	Percent Correct Classification: Best Case (Atmosphere E)
Limonitic Altered	10	20.0 %	30.0 %
Hematitic Altered	87	70.1	79.3
Non-Iron Bearing	13	84.6	84.6
Rhyodacite	15	40.0	40.0
Andesite	29	44.8	58.6
Rhyodacite Ash Flow Tuff	10	60.0	100.0
Rhyolite Ash Flow Tuff	11	54.5	72.7
Anorthosite	20	35.0	20.0
Granite	18	33.3	50.0
Red Sandstone	8	87.5	62.5
Red-Pink Shale-Mudstone	5	60.0	80.0
Basalt	14	64.3	85.7
Coaldale Red Tuff	20	90.0	85.0
Coaldale Light Tuff	61	34.4	37.7
Argillite	12	75.0	66.7
Carbonates (NASA/JPL)	28	42.9	57.1
Carbonate Minerals (ERSIS)	26	76.9	80.8
Carbonate Rocks (ERSIS)	3	0.0%	33.3 %
	Mean	54 %	62 %

FIGURE 19. PREDICTED PERFORMANCE OF THE THEMATIC MAPPER FOR GENERAL GEOLOGIC MAPPING
(Ratio Processing, 390 samples, Channels 1-5+6, 1σ noise)

		1	2	3	4	5	6	7	8	9	10	11	12	13
Channel	1	1.000												
Channel	2	902	1.000											
Channel	3	.778	.956	1.000										
Channel	4	637	872	944	1 000									
Channel	5	492	.729	834	.864	1.000								
Channel	6	.372	.626	742	764	.900	1.000							
Channel	7	.390	.634	.747	.772	892	974	1 000						
Channel	8	.139	.351	.451	.473	568	630	636	1 000					
Channel	9	221	459	.572	.593	.709	776	777	.968	1 000				
Channel	10	.260	.507	622	.647	761	.837	.842	.929	.986	1.000			
Channel	11	186	405	509	531	636	698	700	.958	.978	.967	1 000		
Channel	12	362	616	.736	.756	891	.962	.963	.761	.885	.930	.830	1 000	
Channel	13	.379	.626	746	764	.901	.978	980	.695	834	.889	.766	.990	1 000

FIGURE 20. CORRELATION MATRIX FOR THE THEMATIC MAPPER CHANNELS USED IN THIS SECTION
(Atmosphere E, 1σ Noise Level -- All 441 Samples)

11

CANDIDATE BAND IN THE THERMAL IR REGION

11.1 Introduction, Background

It is assumed that multispectral thermal infrared scanners with more than one channel in the 8-14 μm wavelength region are important for geological remote sensing because the stretching and rotational processes of SiO_4 tetrahedra in silicate rocks and minerals produce emittance minima in this wavelength region which occur at different wavelengths, depending on the mineral composition (R. Lyon 1964). The reasons why emittance minima of the silicate minerals occur at different wavelengths are very complex (see R. Vincent 1975a) and cannot be discussed here. By contrast, vegetation shows nearly a constant emittance in that spectral region and most nonsilicate rocks and minerals exhibit a quite different emittance minima from silicates. For instance, carbonate rocks (limestone, dolomite) have only one rather sharp band near 11.3 μm.

R. Vincent (1973b) has theoretically examined this systematic shift of emittance minima to longer wavelength with decreased quartz content and increased iron and magnesium content. Working with low-altitude aircraft multispectral scanner data he also demonstrated (R. Vincent, 1974 that the optimum filter combination for the purpose of discriminating among silicate rock types on the basis of % SiO_2 and % (SiO_2 - Al_2O_3) was 8.1-10.1 μm for the shorter and 9.2-11.2 μm for the longer wavelength filter. This division of the 8-12 μm region into two thermal channels is supposed to enhance emittance variations in exposed silicate rock outcrops, while suppressing temperature variations across the scene.

From the many results achieved by researchers seeking to exploit the supposed two-channel-thermal IR capabilities for geologic applications only a few will be enumerated:

- using a two-channel thermal IR ratio a rhyolitic tuff was discriminated from alluvium (Vincent 1975a). (This raises the

question whether the unaltered pink rhyolitic tuff mentioned by Rowan et al 1977 could have been separated from altered rocks in the Goldfield area using a thermal IR ratio processing. Because of the great difference in quartz content between these rock types, it is likely, that the tuff and the montmorillonitic-argillic rocks could have been discriminated with a two-channel IR ratio image).

- in general a two-channel IR capability would assist in discriminating alteration zones that are typified by silicification in background rocks of low quartz content and kaolinization from background rocks of high quartz content. The ability to discriminate silicates from nonsilicates would be useful in tungsten exploration.
- two-channel IR ratio processing would permit discrimination between sandstones and limestones or other carbonate rocks as well as quartz sand from calcite sand in beach reconnaissance.
- the mapping of ultrabasic silicates related to diamond-producing kimberlites such as ophiolites should be readily performed with a two-channel IR scanner.
- even sulphates and phosphates, which also have an emittance minimum in this wavelength region and compete with silicates, could be discriminated by ratio processing.

In addition to these geological applications the following reasons for supporting a second thermal IR channel have also been suggested:

- two thermal bands would provide a backup band for thermal information so that if one channel malfunctions, the other could be used for such measurements, even though the two-channel ratio method could no longer be performed.
- by exploiting the differences in emission it should be possible to discriminate dead and dry vegetation.

- thermal band cooling requirements would probably represent less of an increase in the demand upon the sensor support system than that required for a 2.2μm centered band provided the 2nd themal sensor was placed in the same dewar.

11.2 Quantization

11.2.1 Introduction

In order to provide a quantitative measure of the usefulness of a second thermal IR channel for geological application, we began by making use of the ERSIS data. It was not as easy as one might assume to find measured rock spectra in the 8-14μm wavelength region which are mineralogical more or less unequivocal. Unfortunately, we were not able to find as many samples of rock spectra as we would have preferred to support a quantitative study such as this. Also, no comparable study of discrimination between altered and unaltered rocks could be conducted using the thermal region due to lack of appropriate emission spectra. It would have been best to use the same rock samples or at least the same kind of rocks for both the reflective and emissive portion of this study, but this was not possible. Figure 21 shows the different classes which could be established, and the number of individual spectra which each class contained:

Class	No. of Spectra
Acidic Silicate Rocks	47
Intermediate Silicate Rocks	16
Basic and Ultrabasic Silicate Rocks	20
Carbonate Rocks	13
Loams	8
Silicate Mineral & Silicate Sand	4
Hydrothermally Altered Rocks	3
Total Number of Samples	111

FIGURE 21. GROUPING OF ROCK SPECTRA IN THE THERMAL REGION FROM THE EARTH RESOURCES SPECTRAL INFORMATION SYSTEM

11.2.2 Transfer to Space

As explained earlier the radiative transfer model also took into account solar illumination, atmospheric absorption and attenuation in the thermal IR region. For economy we limited ourselves to only one type of atmosphere, namely:

Case B: Tropical atmosphere, visual range = 23 km, sensor view angle = 0°, solar zenith angles = 45°.

Because of the ozone absorption band in the 9.4-9.6 μm region, it was suggested (Vincent, 1977) that the spectral bands be located at 8.2-9.2 μm and 9.8-11.8 μm instead of the overlapping bands from 8.1-10.1 μm and 9.2-11.2 μm which were used in his 1974 study.

11.2.3 Signal/Noise Considerations

This investigation also required that attention be given to the signal/noise characteristics of the Landsat-D Thematic Mapper. We used the following value:

NEΔL = 6.40 μW $sr^{-1}cm^{-2}$ which corresponds to NEΔT of 0.5°K at T=300°K and simulated sensor noise by the procedure presented in Appendix C.

11.2.4 Classification Results

We defined the following three spectral bands for use in the thermal IR study with 111 samples under atmosphere/condition of observation B:

Channel X = 10.4-12.4 μm
Channel Y = 8.2-9.2 μm
Channel Z = 9.8-11.8 μm

The performance of the TM for general geologic mapping using these thermal channels alone is shown in Figure 22 for the case of no sensor noise, and in Figure 23 for the case of 1σ sensor noise. In the configuration where two thermal channels are available, we also show results using ratio processing.

No Sensor Noise -- T=300°K	X	Y & Z	Y/Z
Acidic Silicate Rocks	48.9%	51.1%	25.5%
Intermediate Silicate Rocks	12.5	37.5	31.3
Basic and Ultrabasic Silicate Rocks	10.0	15.0	10.0
Carbonate Rocks	15.4	46.2	61.5
Loams	100.0	100.0	37.5
Silicate Mineral and Silicate Sand	50.0	75.0	75.0
Hydrothermally Altered Rocks	33.3%	66.7%	66.7%

FIGURE 22. PERFORMANCE OF THEMATIC MAPPER THERMAL CHANNELS FOR GENERAL GEOLOGIC MAPPING (NO NOISE)

1σ Sensor Noise -- T=300°K	X	Y & Z	Y/Z
Acidic Silicate Rocks	57.4%	53.3%	21.3%
Intermediate Silicate Rocks	6.3	43.8	12.5
Basic and Ultrabasic Silicate Rocks	--	15.0	55.0
Carbonate Rocks	46.2	46.2	30.8
Loams	100.0	100.0	37.5
Silicate Mineral and Silicate Sand	50.0	75.0	75.0
Hydrothermally Altered Rocks	33.3%	66.7%	66.7%
Mean	42%	57%	43%

FIGURE 23. PERFORMANCE OF THEMATIC MAPPER THERMAL CHANNELS FOR GENERAL GEOLOGIC MAPPING (1σ SENSOR NOISE LEVEL)

Both of these simulations were conducted using the same temperature (300°K) for all the samples. We note that:

(a) the classification accuracy is far below the authors' expectation

(b) the inclusion of a second thermal IR channel did not provide a great increase in classification accuracies.

(c) performance of the ratio processing is disappointingly low in the case of 1σ sensor noise.

(d) the performance which can be expected from a single thermal channel is very limited.

Because the use of a single temperature for all the samples is unrealistic even for observations at 9:30 AM local time, we repeated the simulation with the temperature of each sample drawn from a gaussian distribution. The idea behind this was that for a given scene, there would be no dramatic differences in temperatures from class to class but the samples would range in temperature according to different illumination conditions.

In accordance with this reasoning we drew 111 temperatures from a normal distribution which had a mean value of 300°K and a standard deviation of 5°K. The radiative transfer model was then exercised using one of these temperatures for each sample. The predicted performance of the TM thermal channels under these conditions is shown in Figure 24.

1σ Sensor Noise	X	Y & Z	Y/Z
Acidic Silicate Rocks	21.3%	40.8%	44.7%
Intermediate Silicate Rocks	25.0	56.3	37.5
Basic and Ultrabasic Silicate Rocks	20.0	35.0	40.0
Carbonate Rocks	--	30.8	7.7
Loams	87.5	75.0	12.5
Silicate Mineral and Silicate Sand	0	75.0	75.0
Hydrothermally Altered Rocks	33.3%	33.3%	66.7%
Mean		50%	41%

*Mean sample temperature = 300°K with a standard deviation of 5°K.

FIGURE 24. PREDICTED PERFORMANCE OF THEMATIC MAPPER THERMAL CHANNELS FOR GENERAL GEOLOGIC MAPPING (Random* In-scene Temperatures)

Our interpretation of these results leads to the following statements:

(a) Compared to the performance with two thermal channels, a single thermal channel provides poor results.

(b) For general geologic mapping into these seven classes, two thermal channels gave classification accuracies close to the accuracies achieved by the TM with six reflective channels on the eighteen classes used in Section 10.

(c) The somewhat lower classification accuracies achieved using ratio processing is indicative of the decrease in classification accuracy which should be expected for any preprocessing procedure which accounts for the scene dependent external effects in thermal data.

(d) Further study needs to be made to identify the most effective channels in thermal region for general geologic mapping.

11.3 Conclusions

We emphasize that this thermal study represents no comparable study to the one performed in the 2.2 μm region due to the limited amount of spectra which are available. Incorporation of a 2nd thermal band (8.2-9.2 micrometers) would improve classification accuracies for some general rock types over that obtainable with a single thermal band. Although the present work does not support the contention that accurate identification of rocks according to their SiO_2 content would be possible with two thermal bands, a single thermal band is inadequate to separate variations due to conditions of observation from changes in ground temperatures and emissivities. The authors do not agree with the remark mentioned earlier, by a remote sensing scientist that the implementation of a 2nd thermal IR band would be premature and should wait until experience was gained with Landsat-C data. We fear that although the thermal region contains substantial new information, the difficulties encountered in trying to use a single channel to account for the three competing physical phenomena will introduce more problems than it solves. In addition to these difficulties the current 120 meter ground resolution of the TM thermal band will require great care in the way these thermal data are used in conjunction with the reflective bands during machine processing. Also further studies are recommended to penetrate the relationship between the thermal and reflective region as well as the potential of the thermal region itself for general geologic mapping.

Because the performance of an additional thermal band for general geologic mapping is on the same order as that obtainable with a 2.2 μm band, this candidate spectral band is considered to be a 2nd choice.

12
COMPARISON WITH CURRENT LANDSAT MSS

In order to determine the usefulness of adding different spectral bands to improve the capability given by the present 4-channel Landsat MSS, we ran a study using the same rock spectra collected by NASA/JPL as well as those from the ERSIS. We took into consideration the sensor specification for the current Landsat-II channels and used a linear discriminant analysis with the best case of atmospheric condition (atmosphere E) and a 1σ signal/noise quantization to distinguish altered from unaltered rocks. The following accuracies illustrate the performance which can be expected based upon the classification for 440 of our samples:

Landsat-II MSS	Current TM	Recommended TM
4 Channel	Channel 1-5	Channel 1-5 (+6)
72.5%	79.5%	93.8%

Statements made to us by the GEOSAT committee, confirm that the ability to map zones of altered rocks is very important economically. Hence, the dramatic improvement in classification accuracy for zones of hydrothermally altered rocks gained by incorporating a 2.08-2.35 μm spectral band on the Thematic Mapper justifies its inclusion.

REFERENCES

Abrams, M.J., R.P. Ashley, L.C. Rowan, A.F.H. Goetz, A.B. Kahle, 1977: Use of Imaging in the 0.46 - 2.36 μm Spectral Region for Alteration Mapping in the Cuprite Mining District, Nevada, U.S. Geological Survey Open-File Report 77-585.

Bauer, M.E., L.F. Silva, R.M. Hoffer, M.F. Baumgardner, 1977: Agricultural Scene Understanding, LARS Contract Report 112677, NAS9-14970, Task I.

Bode, D.E., 1976: Infrared Detector Technology-Today and Tomorrow, Electro-Optical Systems Design (EOSD), December 1976.

Condit, H., 1970: The Spectral Reflectance of American Soils, Photogrammetric Engineering and Remote Sensing, September, 1970, pp.955-966.

CORSPERS, 1976: Resource and Environmental Surveys from Space with the Thematic Mapper in the 1980's, National Research Council, Committee on Remote Sensing for Earth Resources Survey.

Del Grande, N.D., 1975: An Advanced Airborne Infrared Method for Evaluating Geothermal Resources, Proceedings of the 2nd United Nations Symposium on the Development and Use of Geothermal Resources, San Francisco, Calif.

EOSPDG, 1973: National Aeronautics and Space Administration, Earth Observation Satellite Payload Discussion Group (EOSPDG) Final Report, Goddard Spaceflight Center, Greenbelt, Maryland.

Gausmann, H.W., D.E. Escobar, E.B. Knipling, 1977: Relation of Peperomia Obtusfolia's Anomalous Leaf Reflectance to its Leaf Anatomy, Photogrammetric Engineering and Remote Sensing, Vol. 43, No.9, September, 1977.

Goetz, A.F.H., F.C. Billingsley, A.R. Gillespie, M.J. Abrams, R.L. Squires, W.M. Shoemaker, A.I. Lucchitta, D.P. Elston, 1975: Application of ERTS Images and Image Processing to Regional Geologic Problems and Geologic Mapping in Northern Arizona, JPL-Report 32-1597

Goetz, A.F.H., 1976: Remote Sensing Geology. Landsat and Beyond, Proceedings of Caltech/JPL Conference on Image Processing Technology, Data Sources and Software for Commercial and Scientific Applications, California Institute of Technology, Pasadena, Calif., pp.8-1.

GSFC, 1977: Specification for the Landsat-D System, GSFC-430-D-100, Preliminary Draft Review Copy, Goddard Space Flight Center, Greenbelt, Maryland.

Halbouty, M., 1976: American Assoc. Petroleum Geologist Bull., N., Vol. 60/5.

Harnage, J. and D. Landgrebe, 1975: Landsat-D Thematic Mapper Technical Working Group, Final Report - NASA/Johnson Space Center.

Henderson, F.B., G.A. Swann, 1976: Geological Remote Sensing From Space, Report of the ad hoc Geological Committee on Remote Sensing from Space with Recommendations for a GEOSAT PROGRAM, Flagstaff, Arizona, Lawrence Berkeley Laboratory University of California, Berkeley, California.

Hoffer, R., 1975: Computer Aided Analysis of Skylab Multispectral Scanner Data in Mountainous Terrain for Land-Use, Forestry, Water Resources and Geologic Applications, NASA-CR-147473; NTIS, N76-19509.

Honeywell Radiation Center, 1974: Multispectral Scanner Data Applications Evaluation, Volume 2, Sensor System Study, NASA JSC-09241.

Hunt, G.R., J.W. Salisbury, 1975: Mid-Infrared Spectral Behavior of Sedimentary Rocks, Air Force Cambridge Research Laboratories, Hanscom AFB, Massachusetts, AFCRL - TR - 75-0356.

Hunt, G.R., 1977: Spectral Signatures of Particulate Minerals in the Visible and Near Infrared, Geophysics, Vol. 42, No.3, pp.501-513.

Ingram, D. and S.G. Wheeler, 1974: EOS-A Final Report, NAS-9-13861.

Kondrat' yev, K.Ya., A.A. Grigor'yev, O.M. Pokrovskiy, 1975: Information Content of the Data Obtained by Remote Sensing of the Parameters of the Environment and the Earth's Resources from Space; NASA Technical Translation, NASA TT F-16435.

Leeman, V., D. Earing, R. Vincent, S. Ladd, 1971: The NASA Earth Resources Sepctral Information System: A Data Compilation, ERIM-Report 31650-24-T, NAS9-9784.

Leeman, V., 1972: The NASA Earth Resources Sepctral Information System: A Data Compilation, First Supplement, ERIM-Report 31650-69-T, NAS9-9784.

Lyon, R.J.P., 1964: Evaluation of Infrared Spectrophotometry for Compositional Analysis of Lunar and Planetary Soils, Rough and Powdered Surfaces, Final Report, Pt 2, NASA Report CR-100.

Marrs, R.W., 1976: Multitdisciplinary Study of Wyoming Test Sites: Type III Final Report for Contract NAS9-13298; University of Wyoming, Dept. of Geology, also available from NTIS, Springfield, Virginia.

Malila, W.A., J.M. Gleason, R.C. Cicone, 1976: Atmospheric Modeling Related to Thematic Mapper Scan Geometry, Final Report NAS9-14819, Task II.

Morgenstern, J.P., R.F. Nalepka, E.R. Kent, J.D. Erickson, 1976: Investigation of Landsat Follow-on Thematic Mapper Spatial, Radiometric and Spectral Resolution, Final Report NAS9-14819.

Nazare, C.V., 1973: An Analysis of Laboratory Hemispherical Reflectance Spectra of Selected Rocks in the Wavelength Range 0.35-2.50 Micrometer, M.S. Thesis, University of Michigan

Nobel, P.S., 1974: Introduction to Biophysical Plant Physiology, W.H. Freeman and Company, San Francisco.

Rowan, L.C., P.H. Wettlaufer, A.F.H. Goetz, F.C. Billingsley, J.H. Stewart, 1974: Discrimination of Rock Types in South-Central Nevada by the Use of Computer-enhanced ERTS-Images, U.S. Geological Survey Professional Paper 883.

Rowan, L.C., A.F.H. Goetz, R.P. Ashley, 1977: Discrimination of Hydrothermally Altered and Unaltered Rocks in Visible and Near Infrared Multispectral Images, Geophysics, Vol 42, No 3, pp. 522-535.

Siegal, B., A. Goetz, 1977: Effect of Vegetation on Rock and Soil Type Discrimination, Photogrammetric Engineering and Remote Sensing, Vol 43, No 2, Feb. 1977, pp. 191-196.

Short, N.M., 1974: Exploration for Fossil and Nuclear Fuels from Orbital Altitudes, GSFS Report X-923-74-322.

Soha, J.M., A. R. Gillespie, M.J. Abrams, D.P. Madura, 1976: Computer Techniques for Geological Applications, Proceedings of CALTECH/JPL Conference on Image Processing Technology, Data Sources and Software for Commercial and Scientific Applications, California Institute of Technology, Pasadena, Calif.

Thomson, F.J., J.D. Erickson, R.F. Nalepka, J.D. Weber, 1974: Multispectral Scanner Data Applications Evaluation, Volume 1, User Applications Study, NASA JSC-09241.

Thomson, F., R. Shuchmann, C. Wezernak, D. Lyzenga, D. Leu, 1976: Basic Remote Sensing Investigation for Beach Reconnaissance, Environmental Research Institute of Michigan.

Tucker, C.J., 1976: Sensor Design for Monitoring Vegetation Canopies, Photogrammetric Engineering and Remote Sensing, Vol 42, No 11, Nov. 1976, pp. 1399-1410.

Tucker, C.J., 1977a): Spectral Estimation of Grass Canopy Variables, Remote Sensing of Environment 6/1977, pp. 11-26.

Tucker, C.J., 1977b): Use of Near Infrared/Red Radiance Ratios for Estimating Vegetation Biomass and Physiological Status, Goddard Space Flight Center, Greenbelt, Maryland; x-923-77-183.

Turner, R.E., 1974: Radiative Transfer in Real Atmospheres, Final Report, ERIM 190100-24-T.

Ungar, S.G., W. Collins, J. Coiner, et al, 1977: Atlas of Selected Crop Spectra, Imperial Valley, California, NASA Institute for Space Studies, NAS5-20749.

Verhoef, W., N.J.J. Bunnik, 1975: A Model Study on the Relations Between Crop Characteristics and Canopy Spectral Reflectance, Netherlands Interdepartmental Working Community for the Application of Remote Sensing Techniques (NIWARS).

Vincent, R., F. Thomson, 1972: Rock Type Discrimination from Ratioed Infrared Scanner Images of Pisgah Crater, California; Science, Vol 175, pp. 986-988.

Vincent, R., 1973 a): The NASA Earth Resources Spectral Information System: A Data Compilation-Second Supplement, ERIM-Report 31650-156-T, NAS9-9784.

Vincent, R., 1973 b): A Thermal Infrared Ratio Imaging Method for Mapping Compositional Variations among Silicate Rock Types, Ph.D. Dissertation, Dept. of Geology and Mineralogy, University of Michigan, Ann Arbor, Michigan.

Vincent, R., 1974: New Theoretical Models and Ratio Imaging Techniques Associated with the NASA Earth Resources Spectral Information System, Environmental Research Institute of Michigan.

Vincent, R., W. Pillers, 1974: Skylab S-192 Ratio Codes of Soil, Mineral and Rock Spectra for Ratio Image Selection and Interpolation, Proceedings of the Ninth International Symposium on Remote Sensing of Environment, pp. 875-896.

Vincent, R., 1975a): The Potential Role of Thermal Infrared Multispectral Scanners in Geological Remote Sensing, Proceedings of the IEEE, Vol. 63, pp. 137-347.

Vincent, R., 1975b): Commercial Applications of Geological Remote Sensing, IEEE Conference on Decision and Control, preprint TA 105, pp. 258-263.

Vincent, R., 1977: Geological Implications of Adding a Seventh Band to LANDSAT-D, Geospectra Corporation, Ann Arbor, Michigan.

Watson, K., 1974: Geothermal Reconnaissance from Quantitative Analysis of Infrared Images; Proceedings of the 9th International Symposium on Remote Sensing of Environment, ERIM, Ann Arbor, Michigan.

Watson, K., 1975: Geological Applications of Thermal Infrared Images; IEEE-Journal, Vol. 63, No 1, pp. 127-128.

APPENDIX A

SPECTRAL FEATURES OF SILICATE AND CARBONATE ROCKS IN THE 2 TO 3 μm REGION

by

George Lindquist

We have done some investigating to try to extract the phenomenology of the spectral features seen around 2.3 μm. I believe the explanation given in three papers by Hunt and Salisbury (Refs. 1, 2, 3) is basically correct, but some of the identifications given there are somewhat misleading. Perhaps a restatement of what is meant is in order, which may serve to put the overall situation in a more physically complete perspective.

I. Silicates

Consider first the water molecule and OH hyrdoxyl complex. The spectrum of the complexes are well known. The water molecule looks like

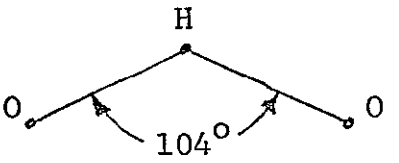

and has 3 modes of vibration: a symmetric stretch at 3654 cm^{-1} (2.74 μm), a bending vibration at 1595 cm^{-1} (6.27 μm), and an assymmetric stretch at 3755 cm^{-1} (2.66 μm). For this bent molecule, all these vibrational modes lead to infrared bands. The OH complex is a simple diatomic and can hence have only one vibrational stretch mode; it is at 3652 cm^{-1} (2.74 μm), right on top of the symmetric stretch vibration of H_2O. Because of this coincidence, it is very difficult to ever see the vibrational fundamental band of OH.

When these molecules are bonded to other atoms or complexes, as in a crystal, their vibrational motion is hindered somewhat (but usually not severely). This leads to a decrease in their vibrational frequencies by a few percent which correspondingly moves their fundamental bands to longer wavelengths by the same percentage. Thus, in liquids and solids we expect to see the same bands from H_2O and OH as we see in the gaseous state, except that, where the orientation of the molecules is fixed, like in an ordered crystal, we expect the bands to be very much narrower than

in gases because no rotational structure will be present. Note that this is not the situation in liquids however, where the molecules are desordered and can interact strongly with each other in a variety of orientations. This leads to much broader bands in liquids than in either gases or crystals.

The bands observed in Ref. 1 at 1.4 and 1.9 μm are due to the H_2O molecules and OH complexes directly. The 1.4 μm band is the first overtone of OH and/or a combination band of H_2O (corresponding to a simultaneous transition in both the symmetric stretch mode and the asymmetric stretch mode). The existence of these combination bands, like the existence of the overtone bands comes about because of non-linear restoring faces in the vibrations and non-linear interactions between the vibrations -- they cannot be explained by the simple springs-and-weights analogy These combination and overtone bands occur in all molecules. The 1.9 μm band is a combination band involving a simultaneous transition in the bending mode and the asymmetric stretch of H_2O. These bands (and a much weaker one at 1.1 μm), as well as the fundamental obscured by atmospheric water vapor at 2.7 μm, are the only bands due solely to water and OH in the spectral range from 1 to 3 μm. The presence of a 1.9 μm band is sure indication of the presence of the H_2O molecule as opposed to the OH complex

Whenever H_2O or OH are attached to other structures, e.g. when an OH replaces an O in a silicate complex, or when H_2O becomes loosely bonded to a molecule in a crystal; other infrared bands become possible. These bands would be combination bands with one or more of the vibrations associated with the structure to which the OH or H_2O is bonded. These other vibrations could be possibly the fundamental of the silicate ion, or possibly vibrations of the lattice structure in which the molecules are arranged or vibrations associated with other degrees of freedom in the crystal. The frequency, and hence wavelength, at which these combination bands appear must correspond to the sum of the frequencies of the modes involved in the transition*.

The persistent bands seen in powdered silicate in Reference 1 at 2.1 to 2.3 μm appear only when OH complexes replace one or more oxygens, at least according to the chemical descriptions included with Ref. 1. This indicates that the bands must be

*This statement assumes that the energy levels of the vibrational modes are equally spaced which is approximately true for the low levels involved at room temperature.

combination bands of OH and some other vibration in the molecules. From the spectral position of the bands and the fundamental frequency of OH, the other moles involved must be between 9 and 14 μm, viz

$$\begin{aligned} 2.1\ \mu m &= 4762\ cm^{-1} \\ \text{OH Fundamental} &= \underline{3652\ cm^{-1}} \\ \text{Other mode} &= 1110\ cm^{-1} \approx 9\ \mu m \end{aligned}$$

or

$$\begin{aligned} 2.3\ \mu m &= 4348\ cm^{-1} \\ \text{OH Fundamental} &= \underline{3652\ cm^{-1}} \\ \text{Other mode} &= 695\ cm^{-1} \approx 14.3\ \mu m \end{aligned}$$

These bands must be combinations between the OH fundamental and some vibrational mode whose fundamental is between 9 and 14 μm. This frequency is too high for lattice vibrations but lies right where one would expect bands of the silicate complex and Al-O bands. The strong quartz (SiO_2) band is right at 9 μm (see Figure 1). The Si-O band, considered as a free complex is at 1247 cm^{-1} (8.05 μm). A fully-bonded SiO_4 silicate ion has a single Si-O stretching fundamental at 555 cm^{-1} (Ref. 5 and 6) (18 μm). Mineral silicates have been shown to have a variety of crystal structures (Ref. 7), in which oxygen atoms are paired with from one to four silicon atoms. Despite the variety of crystal structures we might assume that Si-O stretching fundamentals will all fall between 8.05 μm and 18 μm. On this basis the possible combination bands with OH must all fall between 2.04 μm and 2.37 μm. This is a relatively narrow spectral range and one could postulate that any silicate in which OH replaces one or more of the oxygen atoms will have a band in this range. The replacement of silicon with aluminum and magnesium atoms will modify this situation somewhat, but not greatly; both Al and Mg have masses similar to Si.

The exact spectral position and the fine structure of these OH-silicate combination bands will be indicative of the particular structure of the silicate crystal, including the possible substitution of Mg and Al at the Si sites.

Hunt (Ref. 3) gives a classification of the bands observed in several minerals based on these combination bands and

and combination bands of aluminum and magnesium bearing complexes. I see no reason to doubt his classification at present (see Ref. 3, Figure 8 and pp 508-510).

One can therefore make the following statements about the signature of silicates: A band between 2 and 2.4 μm in a silicate is positive indication of the presence of OH in the silicate. The precise location and structure of the band is indicative of the particular crystal structure. In addition, in the presence of OH, a band will also be present at 1.4 μm. When water molecules are present, bands will be evident at 1.4 and 1.9 μm. Very wide bands, such as are present in Figure 2, are indicative of liquid water rather than bonded molecules These liquid water bands could easily obscure at least the 1.4 μm OH band.

II. Carbonates

The carbonates demonstrate features in the 1.5 μm to 2.5 μm region which are characteristic of the carbonate complex (Ref. 2). The CO_3--complex has a symmetric planar structure. There are six vibrational modes but two are doubly-degenerate, meaning that each of the degenerate frequencies arises from two independent types of motion. The frequencies and motions of the Carbonate complex are shown in Figure 4. Hunt has described the possible combination bands (see Table 1 taken from Ref. 2). In addition he mentions splitting of these bands due to "lifting of the degeneracies" and/or due to long wavelength vibrational frequencies. These two explanations can be taken as identical; the only way the degeneracy could be lost would be by the presence of asymmetric bonds to the CO_3--complex which would indeed manifest themselves in the spectra by combination bands with the vibrations of the CO_3 itself. Thus Hunt's explanations of the carbonate spectra seem quite reasonable. As in silicates details of the carbonate spectra will be indicative of the particular crystals in which the carbonate complexes are involved.

III. Signature Implications

Thus it does appear that both OH-bearing silicates and carbonates will have persistent bands in the 2-2.5 μm region. Furthermore the details of these bands will be dependent on the particular crystal being observed. Unless it is possible to do a very careful analysis of the spectral details I would expect that it would be difficult to reliably distinguish one from the other in remotely gathered images.

References

1. G.R. Hunt and J.W. Salisbury, Visible and Near IR Spectra of Minerals and Rocks, I Silicate Minerals, Modern Geology, Vol. 1, pp. 283-300, 1970.

2. G.R. Hunt and J.W. Salisbury, Visible and Near IR Spectra of Minerals and Rocks, II Carbonates, Modern Geology, Vol. 2, pp. 23-30, 1971.

3. G.R. Hunt, Spectral Signatures of Particulate Minerals in the Visible and Near IR, Geophysics, Vol. 42, pp. 3501-513, 1977.

4. D.R. Stull and H. Prophet, JANAF Thermochemical Tables, Second Edition, NSRDS-NBS 37, National Bureau of Standards, 1971.

5. F. Matossi and O. Bronder, Zeitschrift fur Physik, Vol. 111, p. 1, 1938.

6. G. Herzberg, Infrared and Raman Spectra, Van Nostrand, 1945.

7. L. Bragg, The Crystalline State, A General Survey, Cornell University Press, 1965 Edition.

8. F. Thomson et al., Basic Remote Sensing Investigations for Beach Reconnaissance 108900-5-P, July 1976.

9. W.G. Spitzer and D.A. Kleinman, Infrared Lattice Bands of Quartz, Phys. Rev. Vol. 121, pp 1324-1335, 1961.

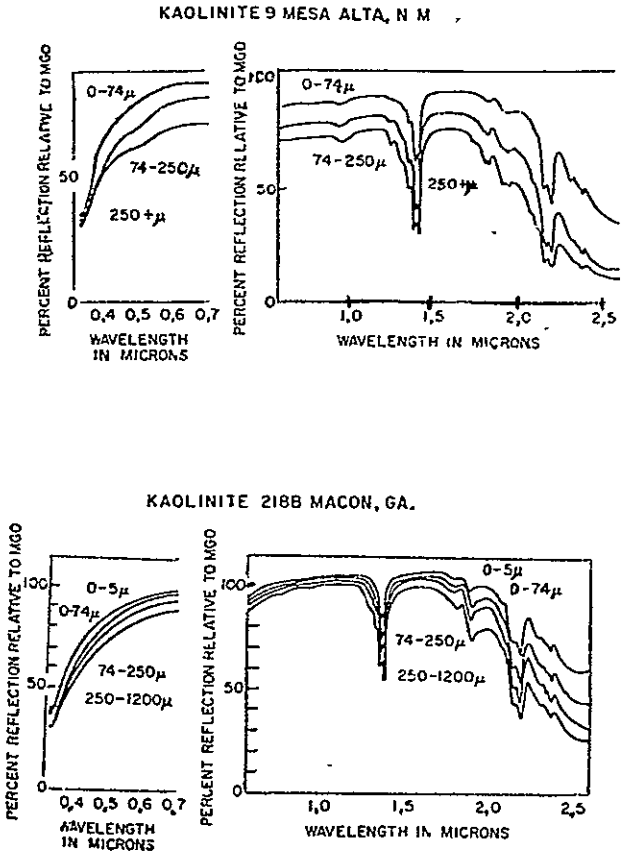

FIGURE 1. SPECTRA OF KAOLINITE POWDERS (TWO SAMPLES) NOTE SIMILARITY OF SPECTRAL DETAILS IN 1.4 and 2.1 μm FEATURES. These details are the manifestation of the crystal structure in the OH and OH-silicate features. The details should be identical on a frequency scale (from Ref. 1).

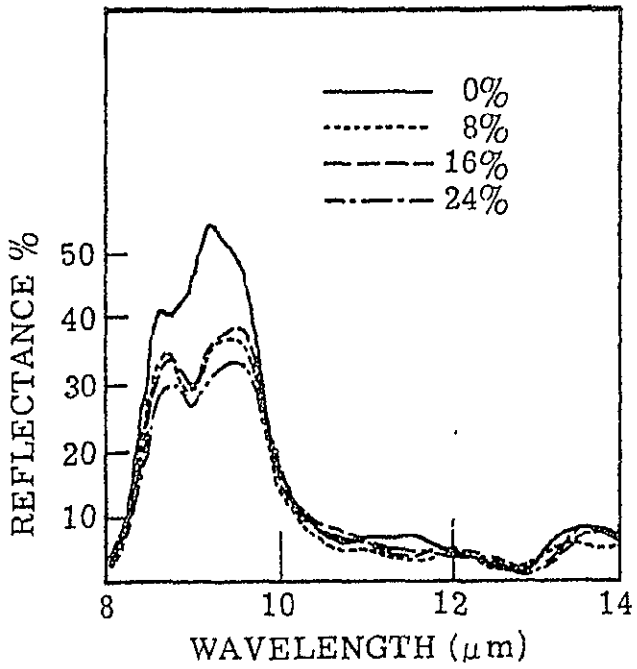

FIGURE 2. REFLECTANCE OF QUARTZ BEACH SAMPLES. The dry spectrum is qualitatively what one would expect (Ref. 9); the small dip at 8.6 μm is a combination band superimposed on the 9.3 μm fundamental (taken from Ref. 8).

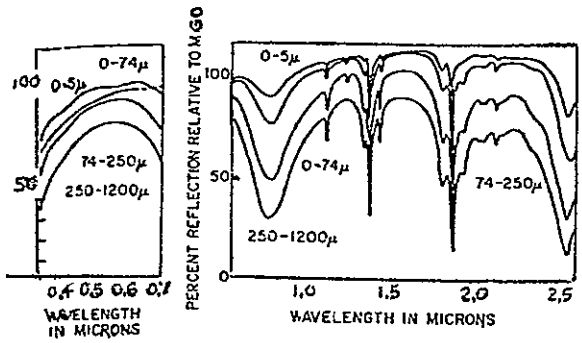

a) Spectra of tightly-bound water molecules.

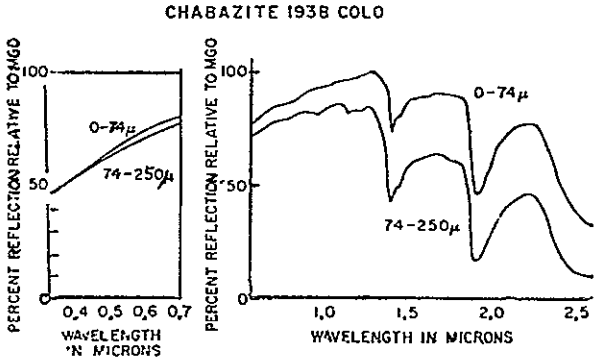

b) Spectra of loosely-bound or liquid water molecules

FIGURE 3. COMPARISON OF SPECTRAL SHAPE OF WATER MOLECULES (FROM REF. 1).

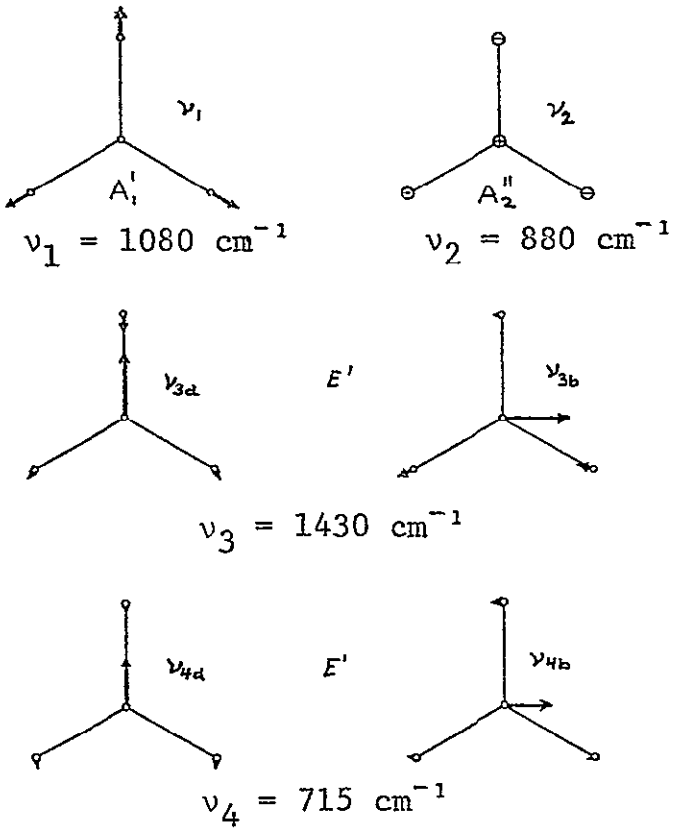

FIGURE 4. ACTUAL FORM OF NORMAL VIBRATIONS IN THE CO_3--COMPLEX (FROM REF. 6).

TABLE I

Band	General position	Assignment	Observed position	Calculated position
I	2.55 μ	$\nu_1 + 2\nu_3$	2.55 μ-2.50 μ sh	2.53 μ
II	2.35 μ	$3\nu_3$	2.35 μ-2.30 μ sh	2.33 μ
III	2.16 μ	$\nu_1 + 2\nu_3 + \nu_2$ or $3\nu_1 + 2\nu_3$	2.16 μ-2.12 μ sh	2.14 μ
			2.16 μ-2.12 μ sh	2.13 μ
IV	2.00 μ	$2\nu_1 + 2\nu_3$	2.00 μ-1.97 μ	1.98 μ
V	1.90 μ	$\nu_1 + 3\nu_3$	1.87 μ-1.85 μ	1.86 μ

(from Ref. 2)

APPENDIX B
CALCULATION OF SENSOR NOISE LEVELS

The physical considerations leading to Eq. (4) and Eq. (5) in the main text are presented in this section.

The reflected radiance is given by:

$$L_R = \rho_1 H_I \ (W\ cm^{-2}\ sr^{-1})$$

where ρ_1 is the bidirectional reflectance (sr^{-1}) of the material

and H_I is the sample irradiance ($W\ cm^{-2}$).

The reflected radiant intensity is given by:

$$I_R = L_R\ A \cdot \cos(\theta_R) = \rho_1 H_I\ A \cos(\theta_R) \ (W\ sr^{-1})$$

where A is the target area (cm^2) and

θ_R is the angle to the reflected ray from the normal to the surface (radians)

Received power is given by:

$$P(R) = (I_R \tau_A + I_{path}) \frac{A_o}{R^2} \tau_o \ (W)$$

where A_o is the area of receiving optics (cm^2)

R is the range between receiver and target (cm)

τ_A is the atmospheric transmission

I_{path} is the path radiant intensity ($W\ sr^{-1}$) and

τ_o is the transmission of the optics

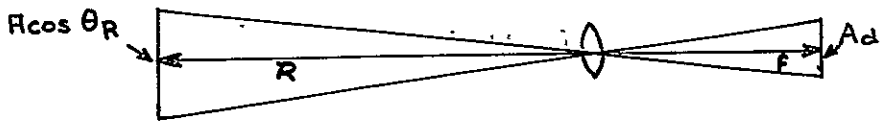

From the geometry illustrated above we see that

$$\frac{A_T}{R^2} = \frac{A\cos(\theta_R)}{R^2} = \frac{A_d}{f^2}$$

where f is the focal length of optical system (cm) and

A_d is the area of the detector (cm^2)

Hence, $\Delta\rho_R$ (reflectance change) $\simeq \Delta\rho_1 \frac{A_o}{R^2} \tau_o \tau_A H_I A_T$

$$= \Delta\rho_1 \tau_o \tau_A H_I A_o \frac{A_d}{f^2}$$

Now, $$\frac{A_o}{f^2} = \frac{\pi D_o^2}{4f^2} = \frac{\pi}{4F_N^2}$$

thus

$$\Delta P_R = \Delta\rho_1 \cdot \frac{\pi}{4} \cdot \frac{\tau_o \tau_A H_I A_d}{F_N^2}$$

Since

$$\rho_1 \simeq \frac{P_d}{\pi}$$

where

P_d is the total diffuse reflectance

we have

$$\Delta\rho_1 \cdot \pi = \Delta P_d$$

and

$$\Delta P_R = \Delta P_d \cdot \frac{\tau_o \tau_A H_I A_d}{4 F_N^2}$$

Hence, the noise equivalent power is given by:

$$NEP = \frac{\sqrt{B\ A_d}}{D^*} \qquad \text{(i.e., Eq. 6 of Section 9)}$$

where B is the electrical bandwidth

and D^* is the detectivity of the detector.

Since $\Delta\rho_d$ corresponds to a signal/noise ratio of one, the noise equivalent reflectance, $NE\Delta\rho$ is given by

$$NE\Delta\rho = \frac{\sqrt{A_d \cdot B}}{D^*} \cdot \frac{4 F_N^2}{\tau_o \tau_A H_I A_d}$$

$$= \frac{4 F_N^2}{\tau_A H_I \tau_o D^*} \cdot \sqrt{\frac{B}{A_d}} \qquad \text{(i.e., Eq. 5 of Section 7)}$$

APPENDIX C

SIMULATION OF SENSOR NOISE THROUGH QUANTIZATION OF INBAND SIGNAL VALUES

There are two, equivalent, ways in which the presence of a random noise component of standard deviation of say 7 μwatts $cm^{-2}sr^{-1}$ could have been simulated.

The first way is to introduce a random noise signal of this magnitude directly on the inband radiance values and repeat the linear discriminant analysis for each atmosphere/condition of observation several hundred times to determine an estimate of the average classification accuracy over the ensemble. We did not use this Monte Carlo technique because of the tremendous computational cost involved.

The second way is based on the observation that what we are seeking is a method to establish a metric in the vector space of the inband radiance values such that one division along any axis corresponds to a noise level of a given probability. For example, at one-sigma noise level the units along each axis should correspond to the levels which can be discerned 68% of the time in the presence of Gaussian noise of say 7 μwatts $cm^{-2}sr^{-1}$.

At first thought quantization into intervals of 7 μwatts $cm^{-2}sr^{-1}$ appears to fulfill this role. However, since the inband radiance values are uniformly distributed over the quantization interval (i.e., any value is equally likely) the standard deviation associated with this procedure is smaller than desired by a factor of $\sqrt{12}$.

Specifically, the standard deviation, σ, of a uniform distribution on the interval, $(\mu - L/2, \mu + L/2)$, is obtained from:

$$\sigma^2 = \int_{\mu-L/2}^{\mu+L/2} 1/L \cdot (x-\mu)^2 \, dx$$

$$= \frac{1}{L} \left(\frac{(x-\mu)^3}{3} \right) \Bigg]_{\mu-L/2}^{\mu+L/2}$$

$$= \frac{1}{L} \left\{ \frac{L^3}{24} + \frac{L^3}{24} \right\}$$

$$\sigma = \frac{L}{\sqrt{12}}$$

Hence, quantization of the inband radiance values into intervals of width equal to $\sqrt{12} \cdot NE\Delta L$ prior to performing the linear discriminant analysis is an equivalent, but a much less costly way to predict sensor performance in the presence of system noise. This procedure is the one we employed in this study.

Technical and Final Report Distribution List

NASA Contract NAS9-15362

NAME	NUMBER OF COPIES
NASA Headquarters 600 Independence Ave., S.W. Washington, D.C. 20546	
Dr. I. Rasool/SS-1	(1)
Mr. Pitt Thome/ERB-2	(1)
Dr. James Morrison/ERD-2	(1)
Dr. Murray Felsher/ER-1	(1)
Ms. Ruth Whitman/ERD-2	(1)
Mr. Mike Calabrese/ERB-2	(1)
NASA/Goddard Space Flight Center Greenbelt, Maryland 20771	
Dr. Vincent V. Salomonson/Code 913 (Landsat D Project Scientist)	(3)
Dr. Louis S. Walter/Code 920	(1)
Dr. A. Rango/Code 913	(1)
Mr. Charles R. Gunn/Code 400.8 (Landsat D Project Manager)	(1)
Dr. Charles Schnetzler/Code 923.0	(1)
Mr. Kenneth I. Duck/Code 720.2	(1)
Dr. Stanley C. Freden/Code 902	(1)
Dr. John L. Barker/Code 923.0	(1)
Dr. Compton J. Tucker/Code 923.0	(1)
Dr. Paul D. Lowman/Code 922.0	(1)
Dr. Nicholas M. Short/Code 923.0	(1)
Mr. Herbert W. Blodget/Code 923.0	(1)
Mr. Oscar Weinstein/Code 726.0	(1)

NAME	NUMBER OF COPIES
NASA/Jet Propulsion Laboratory 4800 Oak Grove Dr. Pasadena, California 91103	
Dr. Alexander F. H. Goetz/Code 183-501	(1)
Dr. Anne B. Kahle/Code 183-501	(1)
NASA/Johnson Space Center Houston, Texas 77058	
Mr. Gene T. Rice/HA	(1)
Mr. Olav Smistadt/HB	(1)
Mr. Richard A. Moke/HC	(1)
Mr. M. Jay Harnage, Jr./HC	(1)
Mr. Gerald P. Kenney/HC	(1)
Mr. Harold E. Granger/HD	(1)
Mr. Robert K. Stewart/HD	(10)
Dr. Robert B. MacDonald/SF	(1)
Dr. Forrest G. Hall/SF	(1)
Dr. Jon D. Erickson/SF3	(1)
Mr. Mickey C. Trachel/SF3	(1)
Mr. William E. Hensley/SF4	(1)
Dr. Phil Weber/SF5	(1)
Mr. Allen L. Grandfield/SF3	(1)
Dr. Richard P. Heydorn/SF3	(1)
Mr. Theodore K. Sampsel/ED6	(1)
Mr. Rex R. Ritz/BB6	(1)
Mr. Ben T. McGuire/BB6	(1)
Ms. Retha Shirkey/JM6	(1)
Mr. Eugene L. Davis, Jr./FM	(1)

NAME	NUMBER OF COPIES
U.S. Geological Survey Federal Center Denver, Colorado 80225	
Dr. Graham R. Hunt	(1)
Dr. J. Taranik	(1)
Mr. H. Curfman, Code 422 NASA/Langley Research Center Hampton, Virginia 23665	(1)
Dr. Fred B. Henderson, III The Geosat Committee 690 Market Street Suite 1400 San Francisco, California 94104	(5)
Mr. Samuel C. Coroniti Office of the Secretary of Transportation Washington, D.C. 20590	(1)
Mr. John Kousandreas Waterside Mall Room 3809 41 M Street, S.W. Environmental Protection Agency Washington, D.C. 20460	(1)
Dr. Gordon Law Assistant and Science Advisor to the Secretary U.S. Department of Interior Washington, D.C. 20242	(1)
Mr. L. P. Murphy ETL-GS-P U.S. Army Engineer Topographic Laboratories Department of the Army Fort Belvoir, Virginia 22050	(1)

NAME	NUMBER OF COPIES
Dr. Charles K. Paul Manager, Remote Sensing Programs Agency for International Development Department of State Washington, D.C. 20523	(1)
Mr. Robin Rowley/HD NASA/Johnson Space Center Houston, Texas 77058	(1)
Mr. Jack W. Sherman, III Chief, Spacecraft Oceanography Group National Environmental Satellite Service National Oceanic and Atmospheric Administration Washington, D.C. 20233	(1)
Dr. George E. Winzer Chief of the Environment and Land Use and Research Group Housing and Urban Development Washington, D.C. 20410	(1)
Mr. George Robcheosky Rainbow Systems 206 N. Washington Street Alexandria, Virginia 22314	(2)
Dr. Clifford Harlan Texas A&M University Remote Sensing Center College Station, Texas 77843	(1)
Dr. Craig Wiegand U.S. Department of Agriculture Soil & Water Conservation Research Division P.O. Box 267 Weslaco, Texas 78596	(1)

NAME	NUMBER OF COPIES
Goddard Institute of Space Studies Columbia University New York City, New York 10025	
Dr. Stephen G. Ungar	(1)
Ms. Vivien Gornitz	(1)
LARS/Purdue University Purdue Industrial Research Park 1200 Potter Drive West Lafayette, Indiana 47906	
Dr. David Landgrebe	(1)
Dr. Marvin E. Bauer	(1)
Dr. Roger Hoffer	(1)
U.S. Geological Survey 1925 Newton Square E. Reston, Virginia 22090	
Dr. Alden P. Colvocoresses	(1)
Dr. John Denoyer Director, EROS Program Bldg. E2	(1)
Dr. Larry Rowan, Mail Stop 927	(1)
Dr. Melvin M. Podwysocki	(1)
Dr. William E. Fischer	(1)
Mr. Stephen J. Gawarecki	(1)
Mr. W. Douglas Carter	(1)
Mr. Moe Deutsch	(1)

NAME	NUMBER OF COPIES
Dr. Robert K. Vincent Geospectra Corporation 320 N. Main Street Suite 301 Ann Arbor, Michigan 48104	(2)
Dr. Floyd Sabins Chevron Oil Field Research Company Standard Oil Company of California, Subsidiary P.O. Box 446 La Habra, California 90631	(1)
Dr. William L. Smith Spectral Data 8100 Cawdorn Port McLean, Virginia 22101	(1)
Dr. Ronald J. P. Lyon Stanford University Palo Alto, California 94305	(1)
Dr. Farouk El Baz Research Director National Air & Space Museum Room 3101 Washington, D.C. 20560	(1)
Mr. Winfred E. Berg National Research Council Committee on Remote Sensing Programs for Earth Resource Surveys 2101 Constitution Avenue Washington, D.C. 20418	(3)